Array imperfection calibration for wireless channel multipath characterisation

JUAN ZHOU

A dissertation submitted in partial fulfillment

of the requirements for the degree of

Master of Philosophy

of

University College London.

Department of Computer Science

University College London

March 14, 2018

I, JUAN ZHOU, confirm that the work presented in this thesis is my own. Where information has been derived from other sources, I confirm that this has been indicated in the work.

Abstract

As one of the fastest growing technologies in modern telecommunications, wireless networking has become a very important and indispensable part in our life. A good understanding of the wireless channel and its key physical parameters are extremely useful when we want to apply them into practical applications. In wireless communications, the wireless channel refers to the propagation of electromagnetic radiation from a transmitter to a receiver. The estimation of multipath channel parameters, such as angle of depature (AoD), angle of arrival (AoA), and time difference of arrival (TDoA), is an active research problem and its typical applications are radar, communication, vehicle navigation and localization in the indoor environment where the GPS service is impractical.

However, the performance of the parameter estimation deteriorates significantly in the presence of array imperfections, which include the mutual coupling, antenna location error, phase uncertainty and so on. These array imperfections are hardly to be calibrated completely via antenna design. In this thesis, we experimentally evaluate an B matrix method to cope with these array imperfection, our results shows a great improvement of AoA estimation results.

Acknowledgements

I would like to express my sincere gratitude and thanks to my supervisor Dr. Kyle Jamieson for the continuous support , his patience, motivation through my study. His help has helped me in all the time. I thank my colleagues in System and Networks group at UCL for their help. My deep gratitude also go to my parents and my husband for their love and support. Finally special thanks to European Research Council for funding much of my graduate studies.

The research leading to these results has received funding from the European Research Council under the European Unions Seventh Framework Programme (FP/2007-2013) / ERC Grant Agreement no. 279976.

Contents

List of Figures

Chapter 1

Introduction

As one of the fastest growing technologies in modern telecommunications, wireless networking has become a very important and indispensable part in our life. Compared with wired networks, wireless networks are easy to install and provide high mobility for users, creating a wide range of applications for enterprise and home networking. Meanwhile, new wireless standards have also brought many types of wireless devices to market, for example, mobile terminals, laptops, and cellular phones. All of these devices not only make our life more convenient but also trigger a lot of practical wireless applications. Thus, a good understanding of the wireless channel and its key physical parameters are extremely useful when we want to apply them into practical applications.

In wireless communications, the wireless channel refers to the propagation of electromagnetic radiation from a transmitter to a receiver [1]. When radio signals arrive at the receivers via a number of paths, we call this phenomenon *multipath*. Multipath is caused by the reflection, scattering and diffraction from the objects such as walls and people in the vicinity of the transmitter and receiver. A typical wireless multipath channel is illustrated in Figure 1.1. A transmitter with one antenna sends a signal to a receiver with one antenna, and the transmitted signal travels over a number of paths before arriving the receiver.

Depending on the transmission bandwidth of the channel as compared to the coherence bandwidth, wireless channels can be categorized into two main groups: *narrowband* and *wideband*. In narrowband channels, the channel frequency re-

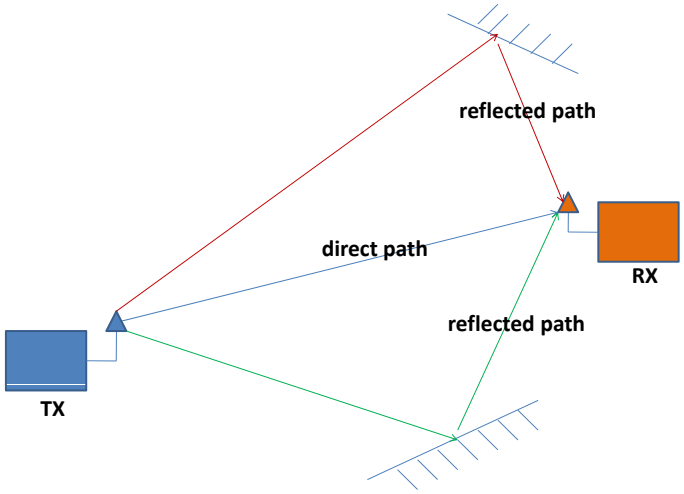

Figure 1.1: Basic concept of multipath wireless channel: signals arrive at the receiver through different paths

sponse can be considered flat over the transmission bandwidth. Though there is no perfect flat fading, the analysis can be greatly simplified if the flat fading can be assumed. However, for wideband channels, this is not the case. A wideband system has a frequency bandwidth that is significantly larger than the coherence bandwidth, thus the frequency response is not flat across the transmission bandwidth. Normally, a wideband system is needed when a high data rate is required.

Due to the existence of multipath, each signal copy will experience differences in attenuation, delay, and phase shift as it travels from the transmitter to the receiver. Depending on the phase shift of each propagation path, signals arriving at receiver antennas can be constructively or destructively combined. When constructively combined, the overall signal strength increases, while if destructively combined, the signal strength is greatly reduced. Strong destructive interference is frequently referred to as a *deep fade*: such a deep fade may result in temporary failure of communication due to a severe drop in the channel signal-to-noise ratio. In wireless systems, multipath induced fading can cause errors and affect the quality of communications. To reduce fading and increase data rates and channel capacity, systems with multiple antennas are often used.

Multiple-input Multiple-output (MIMO): Multiple-input Multiple-output (MIMO) significantly increases channel capacity by using multiple antennas at both

of transmitter and receiver. It has become an important part of modern wireless communication. The technique that MIMO relies on to improve the capacity is spatial multiplexing: making use of spatial dimension to multiplex independent data streams. The spatial dimension of a channel is the dimension of the received signal space, also called *degree of freedom*.

The capacity of a MIMO system with i.i.d. Rayleigh fading channel H is given by [1]:

$$C = \mathrm{E}\left[\log\det\left(\mathbf{I}_{n_r} + \frac{\mathrm{SNR}}{n_t}\mathbf{H}\mathbf{H}^*\right)\right] \text{ bits/s/Hz} \tag{1.1}$$

Where n_r is the number of receiver antennas, n_t is the number of transmitter antennas, SNR is the signal to noise ratio at the receiver antennas, and $\mathbf{H}^*$ denotes the conjugate transpose of the channel matrix $\mathbf{H}$. The standard 2 *2 MIMO example is shown in Fig. 2: Where the transmitter sends packets $x1$and $x2$ simultaneously to

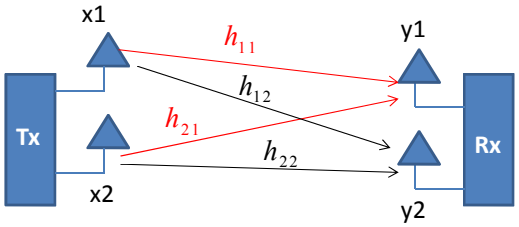

Figure 1.2: Standard 2*2 MIMO system

the receiver, and the receiver hears the following signal:

$$y1 = h_{11}x1 + h_{21}x2$$
$$y2 = h_{12}x1 + h_{22}x2$$

The channel matrix is $\mathbf{H} = \begin{bmatrix} h_{11} & h_{21} \\ h_{12} & h_{22} \end{bmatrix}$. In the wireless MIMO multipath enviorment, each of the channel parameters in the channel matrix needs to be estimated. Though it seems more difficult than the signal antenna system to acquire this information, the multiple antennas actually provide us an useful foundation to use many high resolution spectral analysis techniques.

The estimation of multipath channel parameters, such as angle of depature (AoD), angle of arrival (AoA), and time difference of arrival (TDoA), is an ac-

tive research problem and its typical applications are radar, communication, vehicle navigation and localization in the indoor environment where the GPS service is impractical. The performance of the parameter estimation deteriorates significantly in the presence of array imperfections, which include the mutual coupling, antenna location error, phase uncertainty and so on. These array imperfections are hardly to be calibrated completely via antenna design. Mutual coupling in particular can affect the system in various ways. Mutual coupling is the interactions among antenna elements of an multi element antenna array, one bad effect of the interactions is the distortion of the beam patterns. [2] reports that the mutual coupling at the receive array antennas causes additional correlation between spatial channels and reduces the MIMO system capacity. Besides the mutual coupling, some other impairments such as manufacturing inaccuracies, edge effects of the array and electrical tolerances can also influence the individual antenna elements, making them show up non-uniform amplitude and phase characteristics of the radiation patterns.

In the next chapter, we present the literature review of the technologies that are used to estimate wireless channel parameters and also discuss the different physical array structures and array imperfections. In Chapter 3 we present the system experimental setup and steps used to measure array imperfection. Also a path cancellation technique is used to further improve the parameter estimation results. Then in Chapter 4 we evaluate the B matrix method using our setup in real wireless channel environment and give some experimental results. The conclusion of this thesis is presented in Chapter 5.

Chapter 2

Literature Review

In this chapter, we first survey the different technologies that are used to estimate wireless channel parameters. These channel parameter estimation algorithms can be divided into three basic categories: beamforming-based, subspace-based and maximum likelihood, based on their fundamental principles. We then focus on the discussion of different antenna array designs to see how the physical array structure affects the performance of different estimation techniques.

2.1 Beamforming-based methods

Beamforming-based DoA estimation methods also can be called spatial filter based estimator, because beamforming-based methods form a conventional beam, scan it over the appropriate region and plot the magnitude of the output. The conventional beamformer (BF) or the delay-and-sum beamformer is the simplest method for DoA estimation, the typical estimator is referred to as Bartlett beamformer [3].

The minimum variance distortionless response (MVDR) estimator [4] belongs to beamforming-based estimators, and is also known as the optimum beamformer. It provides an estimation of the power density spectrum over the field of view of an array. To suppress the interference, MVDR uses the adaptively linear filter weights to make sure the signal of interest is undistorted. During the process of optimal weight computation, the two important steps are the computation of inverse correlation matrix and its multiplication with a steering vector. The array correlation matrix is used to determine the spatial filter weights. Compared with the conventional

beamformer, if there is a position error in the antenna, the performance degrades. In [4], the authors study DoA estimation separately for finite sample effects and for small random perturbations in both signal and noise model. The results showed that under certain conditions reducing the dimension of the observation space does not affect the performance of estimator. Also, when the number of snapshots is small, it can also be advantageous.

Though beamforming-based methods are easy and simple to use, they have many limitations. Their estimation accuracy and resolution rely on the physical antenna size, because the antenna main-lobe width is proportional to the physical antenna size.

2.2 Subspace-based methods

Subspace-based methods make use of phased antenna arrays to detect signals. A phased array is an array of antennas in which the relative phases of the respective signals at the antennas is fixed according to the array structure. Relying on the phased antenna array receiver output, these subspace-based methods perform an eigen-analysis of the cross spectral matrix of the output signals and partition the space spanned by the eigenvectors into two subspaces: a *signal subspace* and a *noise subspace*. The steering vectors corresponding to the signal sources in signal subspace are orthogonal to the noise subspace.

2.2.1 MUSIC

Among the subspace-based AoA estimation methods, Multiple Signal Classification [5] (MUSIC) is probably the most studied method. The MUSIC method was first proposed by Schmidt in 1979, and is known as a *super resolution* method compared with traditional beamforming technique whose resolution was limited on the array structure. To understand the idea behind MUSIC, we briefly introduce the data model that MUSIC uses.

Data model: Consider an array of M antenna elements receiving a set of waveforms emitted by D ($D < M$) sources in the far field of the array. Here a narrow-band propagation model is assumed, *i.e.*, the signal envelopes do not change during the

time it takes for the waveforms to travel from one antenna to another. Suppose that the signals have a common frequency of f_0; then, the wavelength $\lambda = c/f_0$ where c is the speed of propagation. The received M-vector X is

$$\begin{bmatrix} X_1 \\ X_2 \\ \vdots \\ X_M \end{bmatrix} = \begin{bmatrix} a(\theta_1) & a(\theta_2) & \cdots & a(\theta_D) \end{bmatrix} \begin{bmatrix} S_1 \\ S_2 \\ \vdots \\ S_D \end{bmatrix} + \begin{bmatrix} N_1 \\ N_2 \\ \vdots \\ N_M \end{bmatrix} \tag{2.1}$$

or

$$X = AS + N \tag{2.2}$$

where X is the received signal at M antenna elements, $\{S_1, S_2, \ldots, S_D\}$ are the incident signals and N represents noise, including the internal noise associated with the radios and external noise coming from the environment. D is the number of source signals, θ_i is the bearing of incident signal i. A is the *array steering matrix*, which represents the relative phase difference between the first antenna (chosen as the reference antenna) and other antennas, as a function of the bearings of incident signals. For example, an uniform linear array (antenna spacing $\lambda/2$), the *array steering matrix* is:

$$\begin{bmatrix} a(\theta_1) & \cdots & a(\theta_D) \end{bmatrix} = \begin{bmatrix} 1 & \cdots & 1 \\ \exp(-j\pi\sin\theta_1) & \cdots & \exp(-j\pi\sin\theta_D)) \\ \vdots & \vdots & \vdots \\ \exp(-j(M-1)\pi\sin\theta_1) & \cdots & \exp(-j(M-1)\pi\sin\theta_D) \end{bmatrix} \tag{2.3}$$

The *array covariance matrix* R for the received signal X is a $M \times M$ matrix as below:

$$\begin{aligned} R_{xx} &= E[XX^*] \\ &= E[(AS+N)(S^*A^*+N)] \\ &= AE[SS^*]A^* + E[NN^*]. \end{aligned} \tag{2.4}$$

In order to further simplify Equation 2.4, MUSIC assumes:

- The incident signals are not correlated with the noise.
- The noise is zero mean and σ^2 variance.
- The number of incident signals D is less than the number of antennas M.

Based on the above assumption, Equation 2.4 becomes:

$$R_{xx} = AR_{ss}A^* + \sigma^2 I, \tag{2.5}$$

Where R_{ss} is the source signal covariance matrix. Eigenvalue decomposition of the array covariance matrix R_{xx} results in M eigenvectors $[e_1, e_2, \ldots, e_M]$ and M corresponding eigenvalues $\lambda_1, \lambda_2, \ldots, \lambda_M$. Sorting the M eigenvalues in non-decreasing order, the first D eigenvalues correspond to the *i*ncident signals, and the $M - D$ eigenvalues correspond to noise. This separates $[e_1, e_2, \ldots, e_M]$ into two subspaces: the *signal subspace* and the *noise subspace*. Since the signal subspace is spanned by the array steering vector of the received signals, the *signal subspace* is orthogonal to the *noise subspace*.

AoA spectrum generation: In [5], the MUSIC AoA spectrum is obtained by converting the Euclidean distance between a steering vector and the *signal subspace* into a function of θ:

$$P(\theta) = \frac{1}{a^*(\theta)E_N E_N^* a(\theta)} \tag{2.6}$$

The denominator of Equation 2.6 becomes zero when θ is the direction of incident signal, and this will yield sharp peaks along the directions of the incident signals when plot the spectrum across all the directions, through the searching for the sharp peaks, AoA of the incident signals can be obtained.

Above is the standard form of the MUSIC method, known as *spectral MUSIC*. it is relatively simple and efficient, but also has limitations, such as a high requirement for the signal-to-noise ratio (SNR), and degraded performance when the incident signals are correlated. Based on this standard form, researchers have

developed many variations to overcome these limitations. We will illustrate them in the following.

2.2.1.1 Root-MUSIC

The standard MUSIC requires high SNR to achieve a good resolution, also it involves a spectral search step which increases the computational complexity. To solve these problems, Arthur [6] presents the *Root-MUSIC* algorithm which finds the roots of the spectrum polynomial and converts the peaks in the spectrum space to the roots of the polynomial lying close to the unit circle.

The steering vector of ULA (suppose the antenna spacing is d) can be written as:

$$a(\theta) = e^{-j2\pi m(d/\lambda)\sin\theta}; \qquad m = 1, \cdots, M \tag{2.7}$$

Substituting Equation 2.7 into Equation 2.6, the denominator becomes:

$$\begin{aligned} P^{-1}(\theta) &= \sum_{m=1}^{M}\sum_{n=1}^{M} e^{-j2\pi m(d/\lambda)\sin\theta} A_{mn} e^{-j2\pi n(d/\lambda)\sin\theta} \\ &= \sum_{l=-M+1}^{l=M-1} c_l e^{-j2\pi l(d/\lambda)\sin\theta} \end{aligned} \tag{2.8}$$

Where $A = E_N E_N^*$, A_{mn} is the entry in the m^{th} row and n^{th} column of A, c_l is the sum of entries of A along the l^{th} diagonal. Then the l^{th} diagonal polynomial representation $D(z)$ is:

$$D(z) = \sum_{l=-M+1}^{l=M+1} c_l z^{-1} \tag{2.9}$$

Now, the evaluation of the MUSIC spectrum $P(\theta)$ is equivalent to the evaluation of the polynomial $D(z)$ on the unit circle. The peaks of the spectrum correspond to the roots of the polynomial $D(z)$. Ideally, the roots of $D(z)$ are located on the positions that are determined by the directions of the incoming signals.

The above process works on a uniformly spaced linear antenna array (ULA). Previous work [6] proved that in low SNR, Root-MUSIC has a higher resolution performance than MUSIC using the example that for two closely-spaced emitters when the SNR is low, the peaks merged together and only showed as one in the

spectrum of MUSIC, thus cannot differentiate the locations of these two emitters. While using the roots of $D(z)$, the roots properly correspond to the correct locations of the emitters. The main limitation of Root-MUSIC is that it only works with uniform linear antenna arrays. This has greatly restricted its usefulness.

To extend to arbitrary non uniform antenna arrays, researchers have designed different methods based on the above process. In [7], the authors propose **interpolated Root-MUSIC**. The main idea is to create a virtual ULA for the non uniform antenna array using linear interpolation, then apply the standard Root-MUSIC method to the output of a virtual ULA. The interpolator coefficients are selected to minimize the interpolation error for signals coming from a given sectors. Through performance evaluation of the interpolated array using both analysis and computer simulation, they find that the interpolation process does not seem to degrade the DoA estimation accuracy when the virtual array is sufficiently close to the real array. However, although this interpolation technique makes it possible to apply Root-MUSIC to arbitrary non-uniform linear antenna arrays, it will make the general two-dimensional array lose the ability to estimate the DoAs in both the azimuth and elevation directions.

A relevant problem of extension to arbitrary antenna arrays is what kind of array geometries will be preferable when using interpolated Root-MUSIC to do DoA estimates. Some papers [8, 9] study the performance of mapped Root-MUSIC. [8] used the approaches called experimental design in statistics, they find that for some realizable nonuniform linear array geometries, applying interpolated Root-MUSIC to virtual ULA will provide better performance than using standard Root-MUSIC to the real ULA with the same aperture length. This finding shows that the performance of interpolated Root-MUSIC is determined by the real antenna array geometry rather than the by the virtual one. They use computer simulations to verify their results.

In [10], the authors study the array mapping (interpolation) combined error, termed as DoA estimate mean-square error (MSE) by taking both bias squared and variance due to noise into account. Compared with [8, 9], it assumes that the inter-

polation errors are negligible compared with the finite sample effects due to noise, extending [11]. In [11], the authors design an algorithm for the mapping matrix is derived by which the resulting MSE could be minimized. They make use of the gradient of a Taylor expansion of the derivative of the DoA estimation cost function. This gradient is used as a tool to quantify, analyze and minimized the bias and variance. They show that DoA bias was not reduced by minimizing the mapping error, but reduced by rotating them into orthogonal to the above gradient. Rotating the mapped noise subspace into an optimal orientation relative to the same gradient can minimize the DoA variance. In [10], the authors derive the first-order expressions for DoA bias, error variance and MSE, formulate a new design algorithm for the mapping matrix to minimize the resulting DoA MSE. A number of simulations are done to study the performance of their proposed MSE-minimizing design algorithm, the results show the MSE minimizing design can be very efficient over a wide range of SNR.

Other extensions of of Root-MUSIC to arbitrary arrays can been found in [12, 13, 14, 15], termed the *manifold separation technique*. This technique is developed from wave field modeling formalism for array processing. The main idea of this technique is to model the steering vector of antenna arrays with arbitrary 2-D or 3-D geometry to be the product of a sampling matrix and a Vandermonde structured coefficient vector. The sampling matrix is only dependent on the antenna array, and the Vandermonde structured coefficient vector is only dependent on the wavefield. Compared with interpolation techniques, MST doesn't need to divide the array into different angular sectors, and has a significantly smaller fitting error over the whole 360^0 area. In addition, MST processes the data directly in element space, so can avoid any transformation or interpolation error. It computes the sampling matrix from array calibration data, which contains information on array imperfections, such as mutual coupling and antenna manufacturing error. However, the calibration data can easily be effected by measurement noise, and so in order to reduce the impact of the noise on the MST, they use effective aperture distribution function, which have been presented in previous papers [16, 17]. The error due to the cali-

bration noise in the modeling of the array steering vector is analyzed, and this error becomes an error floor in the DoA estimates, and dominates over the other random errors. The authors only consider azimuthal angular estimation with the assumption that the noncoherent sources are located in the same elevation angle. In order to verify the proposed error analysis, they simulate these algorithm. The simulation results show that it is possible to predict the performance that can be achieved by subspace-based methods using MST with noisy calibration data.

In [18], the authors present Fourier-domain (FD) Root-MUSIC, an approach that is applicable to arrays with arbitrary geometry. Fourier-domain (FD) Root-MUSIC is based on the fact that the null-spectrum MUSIC function is periodic in angle, and reformulates the DoA estimation using the truncated Fourier series expansion of this periodic function. Because the truncation step can determine the order of FD Root-MUSIC polynomial, the resulting DoA performance is related to truncation errors. High orders of the FD Root-MUSIC polynomial can have the smaller estimation error, but their computation cost may be substantial. Applying the inverse Fourier transform to the FD Root-MUSIC polynomial could avoid this potentially costly computation step. They also propose the further refinement of FD Root-MUSIC using a weighted least-squares approximation of MUSIC null-spectrum to compute the values of Fourier series coefficients. Through simulations with different array configurations, it shows the demonstration that these proposed FD Root-MUSIC algorithms offer attractive alternatives to the above discussed DoA estimation methods applicable to arrays with arbitrary geometries.

2.2.1.2 Spatially-smoothed MUSIC

When the sources are highly correlated due to multipath propagation in practice, MUSIC-based methods can't correctly find the DoA of the each source. The reason why MUSIC-based methods fail when the sources are highly correlated is that the signal covariance matrix becomes singular, and eigen-structure decomposition will fail. Motivated by this problem, researchers introduced the spatial smoothing [19] technique into MUSIC, called Spatially-smoothed MUSIC. This technique is discussed further in [20, 21]. Spatial smoothing is a preprocessing technique which

makes sure the signal covariance matrix will still be nonsingular when the sources are coherent.

The spatial smoothing technique discussed in [19, 20, 21] is designed for an uniformly spaced linear antenna array. Take a M uniformly spaced linear array for example, the M sensors is divided into overlapping subarrays of size M_0, the first subarray has sensors $\{1,\ldots,M_0\}$, and the second subarray has sensors $\{2,\ldots,M_0+1\}$. Denote the kth subarray received signal vector as $X_k(t)$. Then according to Equation 2.2, we can write:

$$X_k(t) = AD_kS(t) + N_k(t) \tag{2.10}$$

Where D_k represents the N x N diagonal matrix

$$D_k = diag\{e^{j\pi d(k-1)sin\theta_1},\ldots,e^{j\pi d(k-1)sin\theta_N}\} \tag{2.11}$$

Then, the coviance matrix of the kth subarray is

$$R_k^f = AD_kR_sD_k^*A^* + E[NN^*] \tag{2.12}$$

The *spatially-smoothed covariance matrix* is defined as the average of the subarray covariances

$$\overline{R^f} = \frac{1}{K}\sum_{k=1}^{K} R_k^f \tag{2.13}$$

where $K = M - M_0 + 1$ is the number of subarrays.

It has been proved [19] that if the number of subarrays is no less than the number of signals ($K \geq N$), then the spatially-smoothed covariance matrix $\overline{R}$ will be nonsingular even when there are some sources are highly coherent or correlated. Since the spatially-smoothed covariance matrix $\overline{R}$ now has the same form as the covariance matrix before preprocessing, the MUSIC-type methods can be successfully applied regardless of the coherence of the sources. The above process is called forward spatial smoothing. However, as discussed [19], there is a trade off between this robustness of spatial smoothed MUSIC and the effective array aperture. With

M sensors array, forward spatially smoothed MUSIC can only resolve $M/2$ signals.

In [20], the authors propose an extension of spatial smoothing, called *forward/backward spatial smoothing*. With forward/backward spatial smoothing, the number of resolved coherent signal can be increased to $2M/3$ with M element antenna arrays. Besides the forward subarrays, it also makes use of another additional K complex conjugated backward subarrays from the same set of arrays to get superior performance. By grouping the sensors at $\{M, M-1, \ldots, M-M_0+1\}$ to form the first backward subarray, and the second one is $\{M-1, M-2, \ldots, M-M_0\}$, etc. Denote $X_k^*(t)$ as the complex conjugate of the received signal of the kth backward subarray for $k = 1, 2, \ldots, K$. Therefore

$$\begin{aligned} X_k^b(t) &= [X_{M-k+1}^*, X_{M-k}^*, \ldots, X_{K-k+1}^*]^T \\ &= AD_k(D_M S(t))^* + N_k(t). \end{aligned} \tag{2.14}$$

The covariance matrix of the kth backward subarray is given by

$$\begin{aligned} R_k^b &= E[X_k^b(t)(X_k^b(t))^*] \\ &= AD_k R_{\bar{s}} D_k^* A^* + E[NN^*]. \end{aligned} \tag{2.15}$$

Where $R_{\bar{s}} = D^{-M} R_s^* (D^{-M})^*$.

The spatially-smoothed backward subarray covariance matrix R^b is defined as the mean of these backward subarray covariance matrices:

$$\overline{R^b} = \frac{1}{K} \sum_{k=1}^{K} R_k^b \tag{2.16}$$

Then the forward/backward smoothed covariance matrix is defined as the average of $\overline{R^f}$ and $\overline{R^b}$:

$$\overline{R} = \frac{1}{2}(\overline{R^f} + \overline{R^b}) \tag{2.17}$$

Because this smoothed covariance matrix $\overline{R}$ has the exact same form as the covariance matrix for standard MUSIC, it can use the subspace-based techniques irrespective of the coherence of the signals. And the authors also give the proof that with at

least 3K/2 sensors, the directions of arrival of K signal sources can be successfully estimated.

In [22], the authors examine the spatial smoothing technique in detail and reveal that the spatial smoothing described above is actually not limited to a uniformly spaced linear array. It can also be applied on arrays which can be divided into subarrays which all have the same structure, but are only shifted with respect to each other, such as a square array. But this is also a strict requirement for the geometries of the arrays. In order to generalize the spatial smoothing technique to arbitrary antenna arrays, [22] proposes to use the output *virtual array* which is created using linear interpolation. Because one can choose the number and configuration of the interpolated arrays, it will have many possible ways to arrange the subarrays to do spatial smoothing. By choosing the suitable number and configuration, the performance can be improved compared with other choices of numbers and configurations. From their analysis, single linear uniformly spaced interpolated array gives the best performance among all three ways of antenna configuration: (a) Interpolated arrays as the shifted versions of real array. (b) Multiple linear uniformly spaced interpolated arrays. (c) Single linear uniformly spaced interpolated array. This interpolation spatial smoothing MUSIC can extend the use of MUSIC-type methods to arbitrary arrays, but its efficiency is not statistical, its performance can be worse in some cases like: the sources are closely spaced. One needs to carefully choose the degree of smoothing, as spatial smoothing inevitably decreases the number of signals it can detect.

2.2.1.3 Beamspace MUSIC

When the array snapshots are passed through a beamforming preprocessor before using MUSIC, the processing technique is called as beamspace MUSIC [23]. Beamspace MUSIC has several advantages compared with the standard MUSIC, such as lower computation, more robust to the system errors and improved resolution. The advantages come from the fact that a number of beams are formed by a beam former, and the number of beams is less than the number of sensors in the array, thus the computation cost is reduced, with less data to be processed.

The signal after the beamspace processor becomes

$$y(t) = W^* x(t) \tag{2.18}$$

Where W is the beamforming matrix. This beamforming matrix consists of beamforming vectors, which form beams toward the expected directions. The beamspace covariance matrix is:

$$\begin{aligned} R_y &= E[y(t)y^*(t)] \\ &= W^* E[x(t)x^*(t)]W \end{aligned} \tag{2.19}$$

Then beamspace MUSIC spatial spectrum can be written as

$$P_{BSMUSIC} = \frac{a^*(\theta)WW^*a^*(\theta)}{a^*(\theta)WT_N T_N^* W^* a^*(\theta)} \tag{2.20}$$

Where T_N is the beamspace noise subspace eigenvector matrix.

In [24], the authors use Root Mean Square Error (RMSE) to evaluate the performance of beamspace MUSIC with the inter-beam angle and source angle.

$$RMSE = \sqrt{\frac{1}{N}\sum_{i=1}^{N}(\theta_i - \theta)^2} \tag{2.21}$$

Where θ_i represents the estimated result at i-th trial. They did the evaluation in two cases, one case was that two sources were inside the beamforming angle, the other one was one source was outside the beamforming angle. The results showed that the RMSE in case 1 is better than case 2.

In [25], the authors study the resolution threshold of beamspace MUSIC for two closely spaced emitters in different scenarios. It is an extension work of [26], It extends the threshold expression in [26] to a more general class of problems, such as arbitrary emitter power level and arbitrary array geometry, then uses the generalized expression to assess the performance of beamspace MUSIC. They demonstrate via analysis that a suitable beamforming preprocessor can significantly reduce the resolution threshold of MUSIC for different two emitter scenarios. Specifically, they

have the conclusions: 1) Using appropriate beamforming preprocessor, the resolution threshold can be reduced by a factor of $(L-2)$, where L denotes the number of sensors. 2) There is no minimum threshold for resolving two closely spaced emitter using the conventional MinNorm algorithm. 3) The beamspace MUSIC and beamspace MinNorm algorithm have the same performance when used with a $L=3$ beamformer for two closely spaced emitters.

2.2.1.4 Frequency-domain MUSIC

The above descriptions of MUSIC operate in the time-domain, which provides a good estimate of DoA. Besides the research of super-resolution techniques in time-domain, researchers have also attempted to use super-resolution techniques in the frequency-domain to estimate other parameters [27, 28, 29].

In [29], the authors propose to apply the super-resolution frequency-domain MUSIC to perform Time-of-Arrival (ToA) estimation for indoor localization. The indoor radio propagation channel is characterized by multiple paths and modeled as a complex low-pass impulse response given by

$$h(t) = \sum_{k=1}^{D} \alpha_k \delta(t - \tau_k), \tag{2.22}$$

where D is the number of incident signals, α_k and τ_k are the complex attenuation and propagation delay of the kth path. Taking the Fourier transform of Equation 2.22, the channel response in frequency domain can be expressed as

$$H(f) = \sum_{k=1}^{D} \alpha_k e^{-j2\pi f \tau_k}. \tag{2.23}$$

α_k and τ_k can be treated as time-invariant in one time snapshot of the measurement.

In practice, a multicarrier modulation technique, such as OFDM (orthogonal frequency-division multiplexing), is used to obtain the discrete samples of the channel in the frequency domain. Then equation 2.23 becomes:

$$H(f_l) = \sum_{k=1}^{D} \alpha_k e^{-j2\pi(f_0 + l\Delta f)\tau_k}, \tag{2.24}$$

where $l = 0, 1, \ldots, L-1$, L is the total number of subcarriers, f_l is the carrier frequency, and Δf is the size of the subcarrier bandwidth. Since noise is present, the measured channel response in frequency domain is given by

$$\overline{H}(f_l) = H(f_l) + w_l = \sum_{k=1}^{D} \alpha_k e^{-j2\pi(f_0 + l\Delta f)\tau_k} + w_l, \tag{2.25}$$

w_l denotes the measured additive white noise. Writing equation 2.25 in vector form, the channel response becomes

$$\overline{H} = H + W = V\alpha + W. \tag{2.26}$$

Where $V = [v(\tau_1), v(\tau_2), \ldots, v(\tau_D)]^T$, $v(\tau_k) = [1, e^{-j2\pi\Delta f\tau_k}, \ldots, e^{-j2\pi(L-1)\Delta f\tau_k}]^T$, and the superscipt T is the matrix transpose operation.

To get the phase changes between different subcarriers, MUSIC needs to do the eigendecomposition of the subcarrier correlation matrix which is computed as

$$R_{HH} = E\{\overline{H}(f_l)\overline{H^*}(f_l)\}. \tag{2.27}$$

The eigenvectors of R_{HH} after eigendecomposition are $E = [e_1, e_2, \ldots, e_L]$: E is divided into a signal subspace E_s and a noise subspace E_n. The time steering vector $v(\tau_k)$ lies in the signal subspace and orthogonal to the noise subspace along the directions of the time of arrival of multipath signals. Then the MUSIC ToA spectrum is

$$P(\tau) = \frac{1}{\alpha(\tau)^* E_n E_n^* \alpha(\tau)}, \tag{2.28}$$

which measures the distance between the time steering vector and the noise subspace.

There are some limitations with this super-resolution MUSIC ToA estimation technique. Although we can decrease τ by choosing a smaller sampling period to increase the resolution of MUSIC, differentiating different paths, resolution is also restricted by the frequency bandwidth of the received transmission and background noise. To overcome this limitation, [30] proposes to combine multiple frequency-

agile transmissions to create a virtual, wider bandwidth transmission, while keep the sampling rate unchanged. Because the resolution of MUSIC ToA estimation is proportional to the bandwidth, the time resolution should scale with the increased bandwidth. Their experimental results show that the resolution of ToA estimation improves significantly.

2.2.2 ESPRIT

ESPRIT [31] stands for **Estimation of Signal Parameter via Rotational Invariance Technique**, it was proposed in 1985 by Roy [32], compared with MUSIC, it is more robust in terms of array imperfections and has less computational complexity since it does not require the extensive search throughout all steering vectors. It requires the sensor array posses displacement invariance, specifically, the sensors in matched pairs need to have identical displacement vectors. ESPRIT not only can estimate the signal parameters efficiently, but also can obtain the optimal signal copy of vectors for reconstructing the signals.

Like MUISC, ESPRIT also assumes that the signals are narrow-band signals, whose signal bandwidth is small compared with the inverse of the transit time of a wavefront across the array, and the array response doesn't depend on frequency over the signal bandwidth. For simplicity, single dimensional parameter space is consider and the sources are far-field. ESPRIT has a constraint on the structure of the sensor array, a planar array of arbitrary geometry was used in [31] to describe this constraint. The elements in each group have identical sensitivity patterns and are separated by a known constant displacement. There are no restrictions on the sensor patterns and positions, each group can have different sensor patterns and its position can be arbitrary.

Data model: Assume D far-field narrow-band sources, an array with M ($D < M$) sensors. The array is composed of two subarrays, Z_X and Z_Y, which are identical expect they are physically displaced from each other by a known displacement vector Δ. The signals received at the i-th group are expressed as

$$x_i(t) = \sum_{k=1}^{d} s_k(t) a_i(\theta_k) + n_{x_i}(t) \tag{2.29}$$

$$y_i(t) = \sum_{k=1}^{d} s_k(t) e^{j\omega_0 \Delta sin(\theta_k)/c} a_i(\theta_k) + n_{y_i}(t) \tag{2.30}$$

Where θ_k is the DoA of k-th source relative to the direction of the displacement vector, which is a reference direction.

The receive data vector can be written as following if combing the outputs of each of the sensors in two subarrays Z_X and Z_Y

$$x(t) = As(t) + n_x(t) \tag{2.31}$$

$$y(t) = A\phi s(t) + n_y(t) \tag{2.32}$$

Where the vector s(t) is the signals of the reference sensor of subarray Z_X, the matrix ϕ is a diagonal matrix of the phase delays between the group sensor for the D signals, and is expressed as

$$\phi = diag\{e^{j\gamma_1}, \ldots, e^{j\gamma_D}\} \tag{2.33}$$

Where $\gamma_k = \omega_0 \Delta sin\theta_k / c$. Because the signals are assumed to be narrow-band. ϕ is a unitary matrix, which relates the measurements from subarray Z_X to those from Z_Y.

The total array output Z(t) is obtained by combing the output of the two subarrays Z_X and Z_Y

$$Z(t) = \begin{bmatrix} x(t) \\ y(t) \end{bmatrix} = \overline{A} s(t) + n_z(t) \tag{2.34}$$

$$\overline{A} = \begin{bmatrix} A \\ A\phi \end{bmatrix}, n_z(t) = \begin{bmatrix} n_x(t) \\ n_y(t) \end{bmatrix} \tag{2.35}$$

The structure of $\overline{A}$ makes it possible to obtain the diagonal elements of ϕ with unknown A. The covariance matrix for Z(t)

$$R_z = E[Z(t)Z^*(t)] = \overline{A} R_s \overline{A}^* + \sigma_0^2 I \tag{2.36}$$

Since there are D sources, the D eigenvectors of R_z corresponding to the D largest eigenvalues form the signal subspace E_s, the remaining $2M-D$ eigenvectors form the noise subspace E_n. Since the span of E_s is the same as the span of $\overline{A}$, there exists a unique nonsingular matrix T such that

$$E_s = \overline{A}T \tag{2.37}$$

Also, because of the invariance structure of the array, the signal subspace E_s can be partitioned into

$$E_s = \begin{bmatrix} E_X \\ E_Y \end{bmatrix} = \begin{bmatrix} AT \\ A\phi T \end{bmatrix} \tag{2.38}$$

E_X and E_Y share the same column space since they are both linear combination of A. Define an matrix, which has rank D

$$E_{xy} = [U_x \quad U_y] \tag{2.39}$$

This implies there exists a unique rank D matrix F such that

$$\begin{aligned} E_{xy}F = 0 \leftrightarrow E_xF_x + E_yF_y = 0 \\ = ATF_x + A\phi TF_y = 0 \end{aligned} \tag{2.40}$$

Based on Equation 2.40,

$$\phi = TF_xF_x^{-1}T^{-1}. \tag{2.41}$$

Define $\psi = F_xF_x^{-1}$, then

$$\phi = T\psi T^{-1} \tag{2.42}$$

Because in practice the measurement is noisy and also includes calibration error, [31] uses a total least-squares (TLS) criterion to estimate the subspace rotation operator ψ. The key relationship in ESPRIT is that: the eigenvalues of ψ are equal to the diagonal elements of ϕ, and the columns of T are the eigenvectors of ψ. The DoA estimation

$$\theta_k = sin^{-1}(c \times arg(\phi_k)/(w_0\Delta)) \tag{2.43}$$

Where ϕ_k is an eigenvalue of ψ.

The above process is an introduction of TLS ESPRIT algorithm in [31]. Compared with [33, 34], [31] uses TLS instead of the standard least-squares (LS) criterion, LS estimators has a restriction on the number of dimensional subspace and potentially has difficulties to extend to generalized eigenproblem. Also, the LS estimators are biased, while TLS estimators are relatively unbiased. However, in some cases when the SNR is sufficiently large, the difference between LS and TLS parameter estimates becomes small. In [31], the authors perform some simulations to compare the performance of ESPRIT with MUSIC. The results show that a bias was presented in the conventional MUSIC, in contrast, ESPRIT estimates are unbiased, but with larger estimate variances because of less information about the array geometry. The estimate variance of ESPRIT decreases when the subarray separation increases and approach as that of MUSIC.

In the original ESPRIT formulation, only one invariance in the array associated with each dimension of the parameter space was assumed, while in many applications, such as a uniform linear array, the array normally has multiple invariance, so which invariance to choose becomes an important question. In [35], the authors present a multiple invariance (MI) ESPRIT algorithm, give a subspace-fitting formulation of the ESPRIT to extend the original ESPRIT to arrays with multiple invariance. With an initial estimate from the standard single invariance ESPRIT, a Gauss-Newton search technique can converge quickly to the desired solution, their results show that normally only one or two iterations is sufficiently to give a solution that is close to the global minimum. They also derive the asymptotic distribution of the estimation error for the MI ESPRIT algorithm and proposed an optimal weighting which can have a asymptotically efficient parameter estimates under certain conditions. Through the simulation, they prove that MI ESPRIT has performance superior to MUSIC, Root-MUSIC and standard ESPRIT, especially in the cases when the sources are highly correlated. MI ESPRIT can also be used in multidimensional parameter spaces problems, such as: the problems with the interest of estimating the azimuth and elevation angles.

In [36], the authors study the problem of extending ESPRIT to sparse array such as nonuniform linear arrays (NLA) which also have multiple invariance. They propose to use a coupled Canonical Polyadic Decomposition (CPD) [37] to reduce the multi-source NLA problems into decoupled single-source NLA problems. By considering the given NLA as a set of superimposed ULA, they can adapt some of the ULA results to NLA. For problems of DoA estimation based on sparse arrays embedded with multiple baselines, the coupled CPD model provided an algebraic framework for sparse array processing. Through their numerical experiments, the results indicate that a good trade off between performance, identifiability, complexity can be obtained by using the multiresolution property of sparse arrays.

2.2.3 JADE

MUSIC and ESPRIT both require that the number of array elements exceeds the number of multipath components. When the number of mulitpath components is larger than the number of array elements, they can not properly estimate the parameters. Also, sometimes, in a multipath scenario, source localization requires not only the DoA, but also the relative delays of each multipath. To solve these problem, Joint Angle and Delay Estimation (JADE) [38] exploits the stationarity of the angles and delays, as well as the independence of fading over many time-slots in a time slotted mobile system, by combining multiple estimates of the channel impulse response over many time slots.

Data model: Just as [38], we start with a single source in a multipath scenario. Let s_i denotes the symbols emitted by the sources with symbol period T, the received baseband data at the i-th element of an array with m sensors.

$$x_i(t) = \sum_{l=1}^{L} \alpha_i(\theta_l)\beta_l(t)r(t-\tau_l) + n_i(t) \tag{2.44}$$

Where L is the number of multipaths, $\alpha_i(\theta_l)$ is the response of the ith sensor to the lth path with the angle θ_l, $\beta_l(t)$ is the fading coefficient of lth path, τ_l is the lth path delay, $r(t) = \sum_i b_i g(t-iT)$, g(t) is the modulated waveform. The received signal

vector x(t) can be written as

$$x(t) = \sum_{l=1}^{L} \alpha(\theta_l)\beta_l(t)r(t-\tau_l) + n(t) \tag{2.45}$$

Where $\alpha(\theta_l) = [\alpha_1(\theta_l), \ldots, \alpha_m(\theta_l)]^T$. If sample x(t) at the symbol rate, we obtain

$$x(k) = Hs(k) + n(k) \tag{2.46}$$

H is the channel matrix including the effects of the array response: delay, symbol waveform and the path fading, it has the form

$$H = [\alpha(\theta_1), \ldots, \alpha(\theta_l)] \begin{bmatrix} \beta_1 & & 0 \\ & \ddots & \\ 0 & & \beta_l \end{bmatrix} \begin{bmatrix} g(\tau_1) \\ \vdots \\ g(\tau_l) \end{bmatrix} =: A(\theta)BG(\tau)^T \tag{2.47}$$

Where $g(\tau_i)$ is a row vector of samples of $g(t-\tau_i)$. Here, the number of multipaths L is assumed to be known, also complex fading is assumed to be constant within a data burst, this is the channel model that JADE uses.

Define h=vec(H) be a vector obtained by taking the transpose of each row of the matrix H and stacking it below the transpose of the previous row, also let $u(\theta,\tau)$ be the space-time vector for a single path of unit amplitude arriving at angle θ with delay τ, given by

$$u(\theta,\tau) =: \alpha(\theta) \otimes g(\tau_i) \tag{2.48}$$

Where $\otimes$ denotes the Kronecker product. If apply the vec$(\cdot)$ operation to 2.47 yields

$$h = (A(\theta) \circ G(\tau))\beta =: U(\theta,\tau)\beta \tag{2.49}$$

Where $\circ$ represents the Khatri-Rao product. $U(\theta,\tau)$ is the space-time manifold matrix and is parametrized by the AoAs and the path delays. In [38], the channel H is assumed to be constant over each time slot, but varies from one time slot to the next. The complex fading β_l changes across different time slots, but the AoAs θ_l

and delays τ_l do not change significantly, so the space-time manifold matrix $U(\theta,\tau)$ stays constant over a few slots. The first step of JADE is to estimate the channel response, which can be achieved using training bits and the least-squares method. Let $\hat{H}$ be the estimates of the channel response H, then

$$\hat{H} = H + V \tag{2.50}$$

Where V is the estimation noise matrix. And obtain

$$\hat{H} = U(\theta,\tau)\beta + V \tag{2.51}$$

The second step of JADE is estimating the $2L$ parameters θ_l and τ_l. Given the matrix $\hat{H}$ and the known structure of the space-time matrix $U(\theta,\tau)$, then seek the desired parameters. There are many methods that can be used in the second step, including Maximum Likelihood and Weighted Subspace Fitting. The reason why JADE can work on the case that the number of antenna is less than the number of the multipath given by [38] is: That $U(\theta,\tau)$ is a tall matrix is required. Their simulations results using JADE-MUSIC and JADE-WSF demonstrate that JADE-based algorithm work successfully in the case that the number of antenna is less than the number of the multipaths.

In [39], the authors propose JADE using shift-invariance techniques. Their algorithm is based on several conditions: 1) The multipaths can be modeled by a discrete number of rays, each parameterized by a delay, complex amplitude and angle. 2) The channel estimate is available. 3) There are no appreciable Doppler shifts and residual carriers of sources. 4) The receiving array is a narrowband phased array, consisting of at least two antennas spaced no more than half wavelength. 5) The received data is sampled at no less than Nyquist rate. There are mainly two steps to estimate the angle and delays, the first step is estimating the channel impulse response from the antenna array, the second step is estimating the angle and delay information using the result of the first step. Shift-invariance techniques were used in the second step, it is much like the 2D ESPRIT algorithm.When they pair

the estimate angle with its corresponding delay, they base on the fact that two matrix of angle and delay have the same eigenvectors, because they share the common factor. The authors find that if two rays have the same delays, then the common factor will become deficient, which leading to the wrong estimation of angles, regards to this problem, they propose to integrate "spatial smoothing" technique with their approach and another method they use is forward-backward averaging, these two approaches are used to extend the data in order to be able to estimate the angles of arrival correctly.

2.3 Maximum-likelihood based Methods

Maximum-likelihood based Methods (MLM) approach the problem as a search for optimal parameters. They estimate DoAs by maximizing a log-likelihood function [40], which is a joint probability density function of the sampled data and is a function of the desired variables, such as DoAs. The maximization of log-likelihood function is a nonlinear optimization problem and requires iterative schemes because it lacks a closed-form solution. The MLM has better performance especially when the SNR is low, the number of samples is small, or the sources are correlated.

In 1968, Kasienski and MsGhee [41] first applied the Maximum-likelihood method to estimate the directions of two plane waves. The results presented show that it is possible to estimate the parameters of targets spaced as closely as a quarter of 3-dB beamwidth, and the accuracy of the estimates depends on the SNR and error level. In [42], Jaffe and Ziskind and Wax propose ML technique for DoA estimation of multiple signals by utilizing the projection matrix to reduce the computational cost. Their simulation results demonstrate that ML has better performance than eigenvector decomposition technique and the Minimum-Energy technique.

Since the maximization of the log-likelihood function requires iterative schemes, followed the previous work on MLM method, researchers present many iterative schemes to make the MLM computationally efficient. These include the well-known gradient descent algorithm [43], alternating projection method [44], the Expectation-Maximization (EM)[40] and Space-Alternating Generalized

Expectation-Maximization (SAGE) [45].

2.3.1 Gradient Descent Method

In [43], the authors extend ML processing to the general case of multiple sources, and derive the Cramer-Rao lower bound on the error covariance matrix. The Cramer-Rao lower bound (CRLB) is an important tool in evaluating the performance of an estimator. The iterative algorithms they propose are gradient descent algorithm which uses the estimated gradient of the function at each iteration as well as the standard Newton-Raphson method. The ML processor consists of beamformers, each focused to a different source, then uses a variable matrix filter which is controlled by the assumed location of the sources. Their results show that when the sources are uncorrelated and the SNR is very low, the processor is simplified greatly and could be seen as the aggregate of ML processors for a single source where each processor is matched to a different source.

2.3.2 Alternating Projection Method (AP)

To reduce the complexity, some works [46, 47] decompose the multidimensional search problem into a sequence of smaller dimensional search problems, and alternating projection (AP) algorithm is one of them.

The AP algorithm is based on an Alternating Maximization (AM) which is a conceptually simple technique for multidimensional maximization. At every iteration, the maximization of AM is performed on a single parameter while all the other parameters are held fixed. Since there exist matrix inversions and multiplications at every iteration, the AM algorithm still has a large computation load. Therefore, AP introduces a projection-matrix update formula into AM to reduce the matrix computation burden. However, since in every iteration, it still needs to compute two Hermitian forms per search point, and normally the number of search points per iteration is far larger when compared to the number of sensor, the complexity per iteration in the AP algorithm is still considerable.

To further reduce the complexity per iteration in the AP algorithm, in [44], the authors present two simple computational algorithms, one is recursive projection

(RP) algorithm, the other is a maximum eigenvector approximation (MEA) algorithm. RP algorithm utilizes the projection matrix update formula to transform the computation of two Hermitian forms into that of only four inner products. MEA algorithm approximates the Hermitian maximization problem to the problem of maximizing the modulus of the projection onto the maximum eigenvector subspace, because of this approximation, the computation of two Heritian forms reduces to only three inner products of vectors, and this doesn't come with any recognizable loss in the performance of estimation and convergence.

2.3.3 Expectation-Maximization (EM)

EM is an iterative approach to Maximum Likelihood estimation. Each iteration is composed of two steps: an Expectation (E) step and a Maximization (M) step. The aim is to maximize the log likelihood in terms of unknown channel parameters of the channel and the receive data. In [48], Feder and Weinstein first introduce the use of EM to find the DoA. The idea is to decompose the observe data into its signal components and then to separately estimate the parameters of each signal component. Below is the an introduction of EM algorithm:
Let Y denote the observed (incomplete) data with the probability density $f_Y(y;\theta)$, and X denote the "complete" data, related to Y by

$$H(X) = Y \tag{2.52}$$

Where $H(\cdot)$ is a nonivertible transformation.

$$f_X(x;\theta) = f_{X/Y=y}(y;\theta) \cdot f_Y(y;\theta) \tag{2.53}$$

Where $f_X(x;\theta)$ is the probability density of X and $f_{X/Y=y}(y;\theta)$ is the conditional probability density of X given $Y = y$, the logarithm of 2.53 is

$$\log f_Y(y;\theta) = \log f_X(x;\theta) - \log f_{X/Y=y}(y;\theta) \tag{2.54}$$

Then taking the conditional expectation given $Y = y$ at parameter $\theta^{'}$

$$\log f_Y(y;\theta) = E\{\log f_X(x;\theta)/Y = y;\theta^{'}\} - E\{\log f_{X/Y=y}(y;\theta)/Y = y;\theta^{'}\} \quad (2.55)$$

For simplicity, define

$$L(\theta) = \log f_Y(y;\theta) \quad (2.56)$$

$$U(\theta,\theta^{'}) = E\{\log f_X(x;\theta)/Y = y;\theta^{'}\} \quad (2.57)$$

and

$$V(\theta,\theta^{'}) = E\{\log f_{X/Y=y}(y;\theta)/Y = y;\theta^{'}\} \quad (2.58)$$

Then Eq. 2.55 becomes

$$L(\theta) = U(\theta,\theta^{'}) - V(\theta,\theta^{'}) \quad (2.59)$$

Using Jensen's inequality

$$V(\theta,\theta^{'}) \leq V(\theta^{'},\theta^{'}) \quad (2.60)$$

if

$$U(\theta,\theta^{'}) > U(\theta^{'},\theta^{'}) \quad (2.61)$$

Then

$$L(\theta)) > L(\theta^{'}) \quad (2.62)$$

2.62 forms the basis for the EM algorithm. The EM algorithm starts with an arbitrary initial guess $\overline{\theta}^{(0)}$, and denotes $\overline{\theta}^{(n)}$ as the estimate of θ after n iterations. Then the next iteration cycle can be described as follows:

E step: compute

$$U(\theta,\overline{\theta}^{(n)}) \quad (2.63)$$

M step: compute

$$\max_{\theta} U(\theta,\overline{\theta}^{(n)}) \rightarrow \overline{\theta}^{(n+1)} \quad (2.64)$$

If $U(\theta, \theta^{'})$ is continuous in both θ and $\theta^{'}$, the iteration converges to a stationary point of the log-likelihood function. The convergence point may not be the global maximum of the likelihood function, hence, several starting points may be needed. The convergence of the algorithm increases exponentially. There are several uncertainties of EM algorithm, such as, multiple choices of transformation $H(\cdot)$ and many possible "complete" data X. The choice of X will critically affect the complexity and the rate of convergence.

Based on EM algorithm, in [48], the authors show that for superimposed signals, there is a natural choice of X, and it decouples the full multidimensional search associated with the direct ML approach into searches in smaller dimensional parameter subspace, significantly reduces the computation cost that is involved. Their results of multipath time-delay and multiple source location estimation demonstrate the performance and the convergence to the exact ML estimate of all the unknown parameters simultaneously.

In [40], the authors propose a generalized expectation-maximization (EM) algorithm for the maximum-likelihood estimation of DoAs of multiple narrow-band signals in noise. Two signal models (deterministic and stochastic) are considered. Their work was an extension work of [48], but differs in the following ways: 1) They focus on narrow-band case and assume the signal waveforms are unknown, thus need to jointly estimate the directions and the signals. 2) They generalize the EM algorithm for solution of the deterministic signal model. 3) They show through simulation that convergence is achievable when the initial angle estimate are within about one bandwidth of the global maximum. Their results also demonstrate EM algorithm is not sensitive to initial conditions on the signal powers, but the initial angle values are the crucial parameters. In addition, they incorporate prior knowledge of the signal structure, which has a significant effect on the angle estimator performance under the deterministic signal model.

2.3.4 Space-Alternating Generalized Expectation-Maximization (SAGE)

Classical EM maximizes the conditional log likelihood of the unobservable complete data space, rather than for the measured or incomplete data, it updates all the parameters at the same time, causing slow convergence and difficult maximization steps. To improve these drawbacks of EM, the authors [45] propose SAGE. The SAGE algorithm updates parameters sequentially by replacing the high dimensional optimization process necessary to compute the joint maximum likelihood estimate of the parameters, by several separate, low dimensional maximization procedures, which are performed sequentially. SAGE is suited to problems where one can sequentially update small groups of the elements of the parameter vector, instead of using one large complete-data space. Each group of parameters is associated with a hidden data space which shows as a complete-data space if all the other parameters are known. However, compared with EM, SAGE is less amenable to a parallel implementation because it is coordinate wise method. They also demonstrated that SAGE algorithm improved the asymptotic convergence rate, although the actual convergence rate depended on how close the initial estimate is to a fixed-point.

In [49], the authors use a linear array to evaluate SAGE through extensive Monte-Carlo simulations and in real propagation environment. Their simulation results show that SAGE can rapidly converges in synthetic discrete propagation environment given that the waves are well resolvable with respect to their delays and incidence directions. If they are not well resolvable, the convergence is slower. In a real environment, the experiment results also demonstrate the feasibility of SAGE.

2.4 Antenna array structure

When we review the methods to estimate the multipath parameters, we cannot ignore the effects of the arrays with different geometries. Antenna arrays are becoming increasingly important in wireless communication. A signal wavefront which propagates across the array of antennas is picked up by all antennas. Thus, we have many outputs which constitute an array signal. Sometimes, all components of the

array signals are simply delayed replicas of a signal waveform. but sometimes, each individual antenna outputs is strongly corrupted with noise and other interference, making the signals are quite different among them. Array processing now involves combining all sensor outputs in some optimal manner so that the coherent signal emitted by the source is received and all other inputs are maximally discarded. The aperture of an array (that is, the spatial extent of the array distribution) is a limiting factor on resolution.

2.4.1 Uniformly spaced antenna array

Uniformly spaced antenna arrays mean arrays have a constant spacing among elements, includes 1D, 2D or 3D arrays. In application, the maximum spacing is a half wavelength to avoid grating lobes, which means two distinct DoAs produce the same set of phases across the array. The most commonly used array geometries are uniform linear array (ULA) and uniform circular array (UCA). The ULA has excellent directivity and it can form the least main-lobe in a given direction, but it is difficult to be kept consistent in large range and do not treat equally all azimuths [50]. UCA is high side-lobe geometry so the distance of array antenna should be small and the basic symmetry of circular arrays offers a great ability to compensate for the effects of mutual coupling.

2.4.1.1 Uniform Linear Array (ULA)

Uniform linear arrays are arrays that have the same array elements and these array elements align along a straight line with equal spacing. The array weight vector

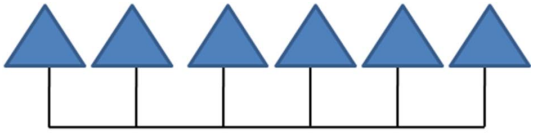

Figure 2.1: Uniform Linear Array (ULA)

(supposing the amplitude is I and the phase difference between adjacent elements

is β) is

$$W = \begin{bmatrix} w_1 \\ w2 \\ \vdots \\ w_N \end{bmatrix} = \begin{bmatrix} Ie^{j\beta} \\ Ie^{j2\beta} \\ \vdots \\ Ie^{j(N-1)\beta} \end{bmatrix} \tag{2.65}$$

The array factor (AF) for this array specified on the plane $\theta = \pi/2$ is

$$\begin{aligned} AF &= f_{array}(\theta = \pi/2, \phi) \\ &= \sum_{i=1}^{N} w_i e^{jb_i} \\ &= \frac{\sin(N\frac{\psi}{2})}{\sin(\frac{\psi}{2})} e^{j(N-1\frac{\psi}{2})} \end{aligned} \tag{2.66}$$

where $\psi = kd\cos\phi + \beta$ and $0 \leq \phi, \beta \leq 2\pi$. $|AF|$ is the normalized antenna factor, it is a periodic function of ψ, with a period of 2π, also is symmetric about the line of the array.

ULA has the simplest antenna array geometry, many super resolution DoA estimation method are developed based on it. But because of the symmetry of $|AF|$, it can only provide a 180-degree angle scan.

2.4.1.2 Rectangular Array (RA)

If N ULA arrays are placed next to each other in the y direction, a rectangular array will be formed. Assume that they are equally spaced at a distance of d_y and there is a

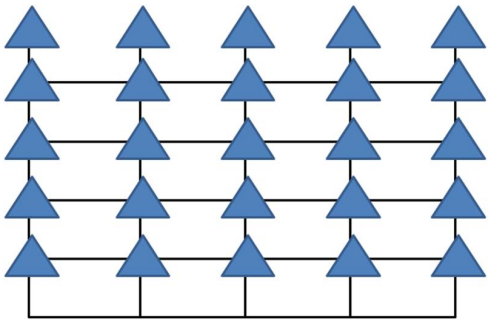

Figure 2.2: Rectangular Array (RA)

progressive phase difference along each row of β_y, also assume that the normalized

current distribution along each of the x-directed array is the same but the absolute values correspond to a factor of I_{1n} (n=1,$\cdots$,N). Then the array factor (AF) of the rectangular array is

$$AF = \sum_{n=1}^{N} I_{1n}[\sum_{m=1}^{N} I_{m1} e^{j(m-1)(kd_x sin\theta cos\phi+\beta_x)}]e^{j(n-1)(kd_y sin\theta cos\phi+\beta_y)} \tag{2.67}$$

For simplicity, 2.67 can be written as

$$AF = S_{x_M} \cdot S_{y_N} \tag{2.68}$$

Where $S_{x_M} = \sum_{m=1}^{N} I_{m1} e^{j(m-1)(kd_x sin\theta cos\phi+\beta_x)}$ and $S_{y_N} = \sum_{n=1}^{N} I_{1n} e^{j(n-1)(kd_y sin\theta cos\phi+\beta_y)}$
The pattern of a rectangular array is the product of the array factors of the linear arrays in the x and y directions. To avoid grating lobes, the spacing between the elements must be less than λ ($d_x < \lambda$ and $d_y < \lambda$).

2.4.1.3 Uniform Circular Array (UCA)

Uniform circular arrays are commonly used when 360 degree coverage is required in the plane of the array. Compared with ULA, UCA can provide a 2D angular scan, both horizontal and vertical scans. In addition, distortions in the array pattern of a circular array due to mutual coupling effect are same for each element, so it would be easier than ULA to deal with the mutual coupling effect.

For a uniform circular array with N elements and equal amplitude I and a

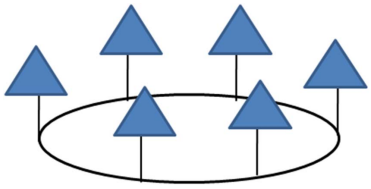

Figure 2.3: Uniform Circular Array (UCA)

current phase of β_n (reference to the central point of the array) for the nth element ($\phi_n = 2\pi n/N$), the array factor is

$$AF = \sum_{1}^{N} e^{j[kasin\theta cos(\phi-\phi_n)+\beta_n]} \tag{2.69}$$

In UCA, a desired maximum radiation direction is first chosen, then we compute the excitation phase for each element. The computed phase may not be equally increasing from one element to the next, which is different from the case of a linear array.

However, since they are non uniform linear arrays, many high resolution DoA estimation methods like the methods discussed above can not be directly used on UCA. Researchers have presented many methods to convert a UCA into a virtual ULA in order to apply high resolution DoA estimation methods.

2.4.2 Non-uniformly spaced antenna arrays

Non-uniformly spaced antenna arrays can be arrays with the arbitrary geometry. The location of the nth antenna element can be described by the vector d_n, where

$$d_n = [x_n, y_n, z_n] \tag{2.70}$$

The set of locations of an N-element antenna array will be described by a N-by-3 matrix D, where

$$D = \begin{bmatrix} d_1 \\ d_2 \\ \vdots \\ d_N \end{bmatrix} \tag{2.71}$$

For non-uniform spaced antenna array, it is generally more difficult to estimate the DoAs using super high resolution. But researchers have developed many variations of these super high resolution methods to meet the requirement of estimating DoAs for arrays with arbitrary geometry.

2.4.3 Array Imperfections

Compared with ULA (uniform linear array), UCA(uniform circular array) can provide a 360 degree angular scan, thus it is a natural choice for our system. However, in realistic cases, UCAs usually suffer from mutual coupling and geometrical perturbations. All these array imperfections can decrease the accuracy of AoA estimation.

Mutual coupling: When the antenna spacing of UCAs is less than half of the wavelength, the mutual coupling is usually present. Mutual coupling in an antenna array is the electromagnetic interaction between the antenna elements. It will be serious when the element spacing is small. The mutual coupling can affect the antenna parameters like input impedance, reflection coefficients, hence these effects will change the array radiation pattern (for transmit antenna array) and the array receive manifold (the received signal at the receive antenna array). Because the estimation of AoA of UCA is based on the received signal at all antennas, the estimation results will be inevitably affected.

Other array imperfections can also have a bad effect on the AoA estimation, such as non-omnidirection, non-identical elements, and deviations of the array elements from their nonminal locations. To cope with these array imperfections, in [51], the authors propose to use a preprocessing technique, which can be referred as a B matrix method:

$$\mathrm{B}\alpha(\theta) \approx \tilde{\alpha}(\theta) \tag{2.72}$$

To estimate B, let A and $\widetilde{\mathrm{A}}$ denote, respectively, the matrices of the steering vectors of the actual and ideal array manifolds,

$$\mathrm{A} = \left[\alpha\left(\theta^{(1)}\right), \ldots, \alpha\left(\theta^{(L)}\right)\right] \tag{2.73}$$

and

$$\widetilde{\mathrm{A}} = \left[\tilde{\alpha}\left(\theta^{(1)}\right), \ldots, \tilde{\alpha}\left(\theta^{(L)}\right)\right] \tag{2.74}$$

The estimation of B is based on the least squares criterion and B as the matrix that minimizes the following expression:

$$min||\widetilde{\mathrm{A}} - \mathrm{BA}||^2 \tag{2.75}$$

The solution is:

$$\hat{\mathrm{B}}^H = (\mathrm{AA}^H)^{-1}\mathrm{A}\widetilde{\mathrm{A}}^H \tag{2.76}$$

After obtaining B, we can use it to compensate the imperfections, the receive signals after compensation are given by:

$$x(t) = \hat{\mathrm{B}}x(t) \tag{2.77}$$

Chapter 3

Methodology

The goal of our work is to find the accurate B matrix and use it to deal with array imperfections, in order to improve the estimation of path parameters including Angle of Arrival (AoA). The system setup includes one client with two antennas and one AP with 8 element Uniform Circular Antennas. At the receiver side, we use MUSIC to estimate the Angle of Arrival (AoA) of the paths.

3.1 Hardware

The hardware platform we use is Rice WARP [52] with WARPLab version 7.3. One WARP is used as the transmitter, and two WARPs are synchronized to act as a receiver (AP). Each WARP is attached with the FMC-RF-2X245 module to enable four radios on each board. So in order to make an eight radios system, two WARPs need to be synchronized use time and frequency synchronization module. For receiver, the antenna array we use is a fidelity UCA with 8 antennas as shown in Figure 3.1. Coaxial cables are used to connect the antennas to the WARP radios. All the data received at the APs are transmitted to server through Ethernet connection between the WARPs and the server. The AoA estimation algorithm is implemented at the server.

3.2 B matrix measurement

For measurement of actual array manifold, the antenna array has to be placed inside an anechoic chamber as shown in Figure 3.2 to avoid the interferences from

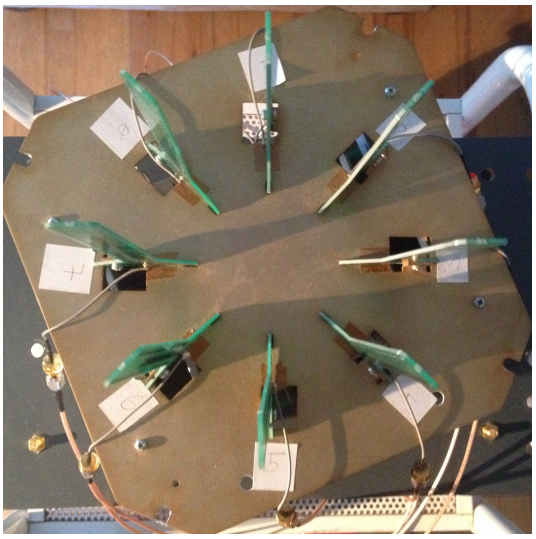

Figure 3.1: UCA

reflected paths. Anechoic chamber is a room designed to absorb the reflections of sound and electromagnetic waves and insulated from exterior sources of noise. There are different sources of error that may come up if we don't take care of it, such as: the device in the anechoic chamber, the unshutted door. Also, the calibration of WARP before measurement may cause the potential estimation error. In order to get the most accurate result, we did the following thing to eliminate the error. (a) We cover every device which was placed in anechoic chamber with the absorbing materials. (b) For the wires that need to be pulled out to connect the computer outside the anechoic chamber, we use the holes in anechoic chamber wall insteading of directly pulling them out from the door, in this way, we can make sure the door will be shut properly. (c) For receiving WARP, we did multiple calibrations to verify that we have correctly done the calibration. The setup of the experiment is: one antenna transmits signal and an 8 element uniform circular array shown in Figure 3.3 receives signal. The detailed steps are as below:

(1). Do wired calibration for two receiving warps (for both phase and magnitude) to eliminate the phase and magnitude differences among different antennas at the receiving antenna array.

(2). After the calibration, start to transmit and receive data in wireless environment. In order to get the full 360 degree position data, the transmit antenna has been put

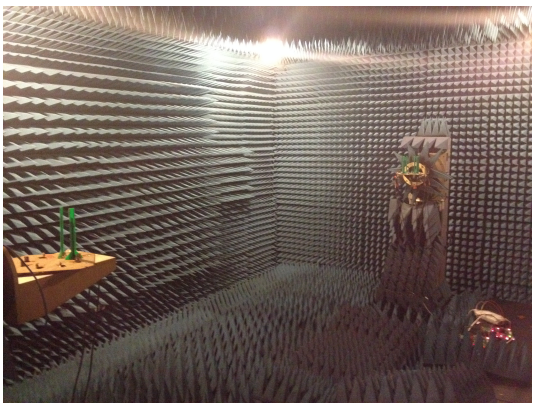

Figure 3.2: anechoic chamber

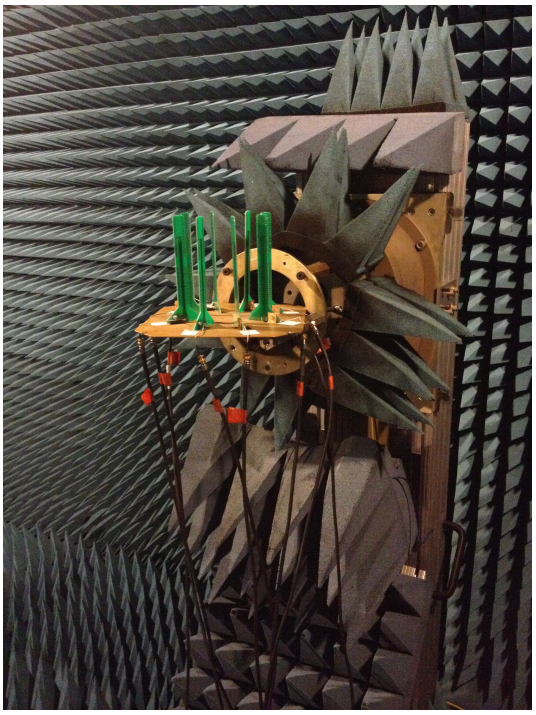

Figure 3.3: 8 antenna UCA in anechoic chamber

on the turning table, and the turning table will move in every 1 degree step from 1 degree to 180 degree. To get 180 degree to 360 degree, we need to flip the receiving UCA.

(3). For the receive signal at each position: (a) Apply phase and magnitude compensation to the raw receive data. (b) Save the raw receive data.

(4). Repeat step (3) for each position, now total we have 360 position data. For every position data, compute the relative receive data (divide the reference antenna receive data), then put all these data into a matrix to form A according to the above method. The dimension of A is 8*360.

(5). Compute B matrix and compensate the receive signals.

We use the method in [51] to compute B matrix method:

$$\hat{\mathrm{B}}^H = (\mathrm{A}\mathrm{A}^H)^{-1}\mathrm{A}\widetilde{\mathrm{A}}^H \tag{3.1}$$

Where A and $\widetilde{\mathrm{A}}$ denote, respectively, the matrices of the steering vectors of the actual and ideal array manifolds,

$$\mathrm{A} = \left[\alpha\left(\theta^{(1)}\right), \ldots, \alpha\left(\theta^{(L)}\right)\right] \tag{3.2}$$

and

$$\widetilde{\mathrm{A}} = \left[\tilde{\alpha}\left(\theta^{(1)}\right), \ldots, \tilde{\alpha}\left(\theta^{(L)}\right)\right] \tag{3.3}$$

3.3 Interference cancellation

In order to get a better estimation result for each path when we perform the experiments in real enviroments, we also use interference cancellation technique to cancel all the other paths expect the one we are interested in. In order to do the cancellation, we first use MUSIC to get all the AoAs, then we pick up the angle we want to keep, and use Gram-Schmidt orthogonalization to project the raw receive signal to the signal space which is orthogonal to the angle we keep. We can repeat this method for each path that we are interested in. After the cancellation of all the other paths from the raw receive signal, we can apply MUSIC on this more cleaned signal

to get a more accurate AoA results.

Chapter 4

Evaluation

To show how well the results are, we present some experimental results and simulation results as below. First, to evaluate the accuracy of the B matrix, we apply the B matrix back to the raw receive data we gathered at the anechoic chamer, this way can make sure the results won't be affected by the reflected paths. We present the improved AoA results of B matrix compensation for uniform circular array imperfection. After that, we demonstrate that the interference cancellation technique is robust against the different signal strength levels, also show good results for real experiments.

4.1 B matrix compensation

We first show the AoA results for some positions before using B matrix to compensate the array imperfection. Fig 4.1 and Fig 4.2 are the AoA results of position 1 to 110 at every 10 degree and position 120 to 230 at every 10 degree. We can see that the angle estimations are roughly accurate, with the estimation error less than 2 degree, but the width of the peaks are wide, which could be caused by the array imperfections. Wide peak can seriously make the AoA estimation results wrong when there are more than peaks appear in real wireless environment, because these peaks will start to merge together if each of them is wide.

Next, we will show some AoA results after the B matrix compensation. To evaluate the B matrix, we first apply the B matrix back to the raw received signals which are used to compute the B matrix, we expect to see that there is a great im-

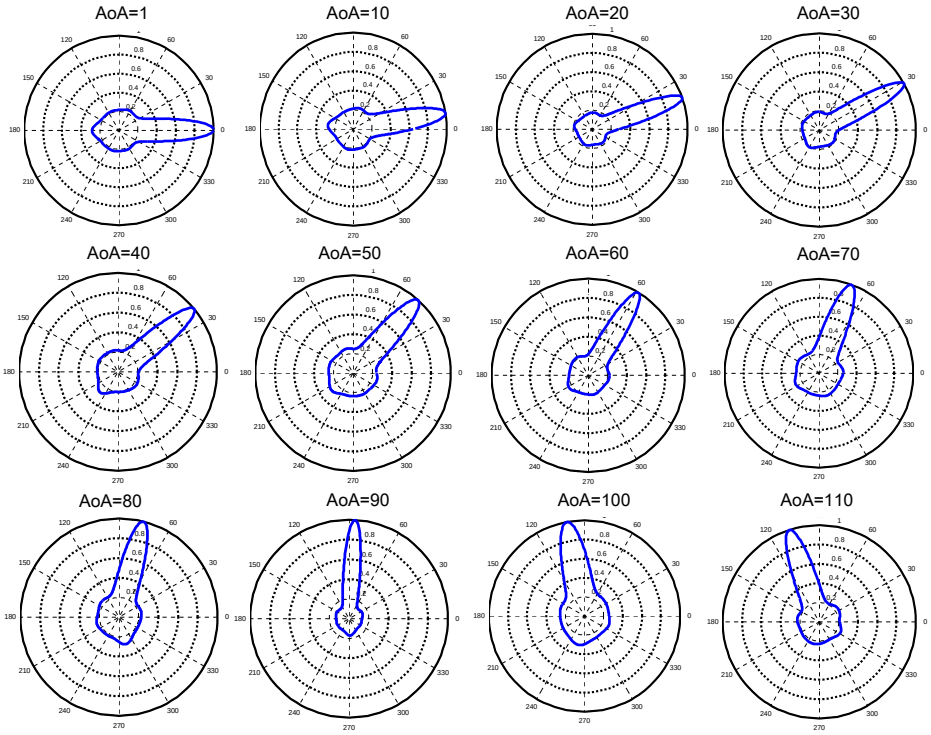

Figure 4.1: AoA results before using B matrix compensation (Position 1 to 110 at every 10 degree)

provement for every position. Fig 4.3 and Fig 4.4 are the AoA results of position 1 to 110 at every 10 degree and position 140 to 250 at every 10 degree. It is obvious that the width of the peak has become smaller than before. However, we also find that after B matrix compensation works better for some positions than some other positions. For position 25 degree, Figure 4.5 is the AoA result before using B matrix, and Figure 4.6 is the AoA result after using B matrix, It is clearly that the AoA after B matrix compensation has become sharper than the AoA before applying B matrix. For position 264 degree, Figure 4.7 is the AoA result before using B matrix, and Figure 4.8 is the AoA result after using B matrix, we can see that the angle has improved, but the width of the peak doesn't have much improvement as position 25 degree.

The reason of the difference between different positions could be the hardware imperfection. Because the B matrix is computed using the data at all the

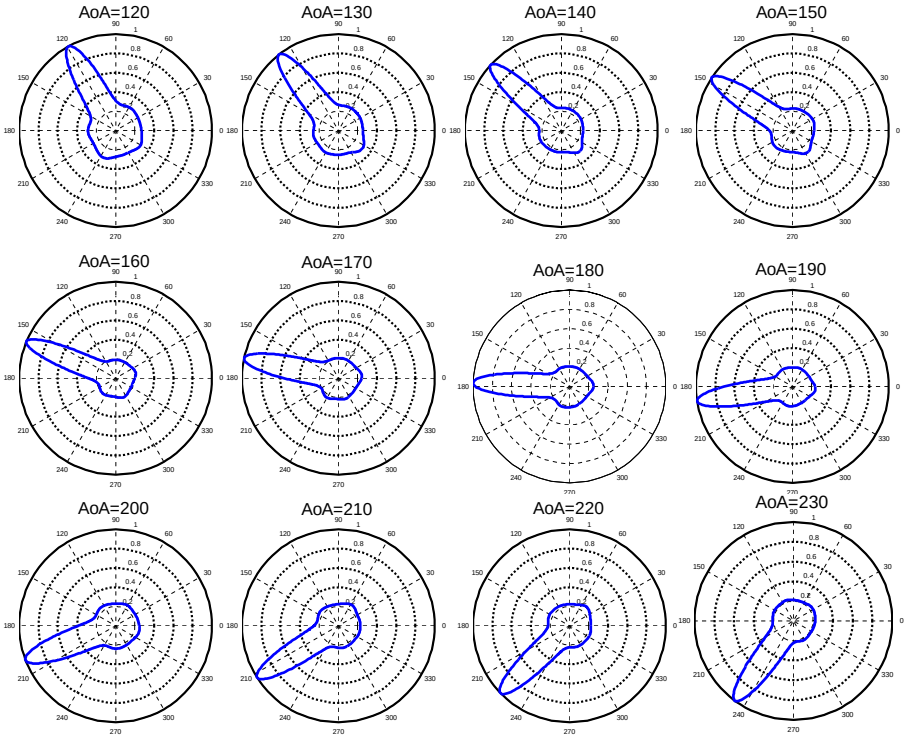

Figure 4.2: AoA results before using B matrix compensation (Position 120 to 230 at every 10 degree)

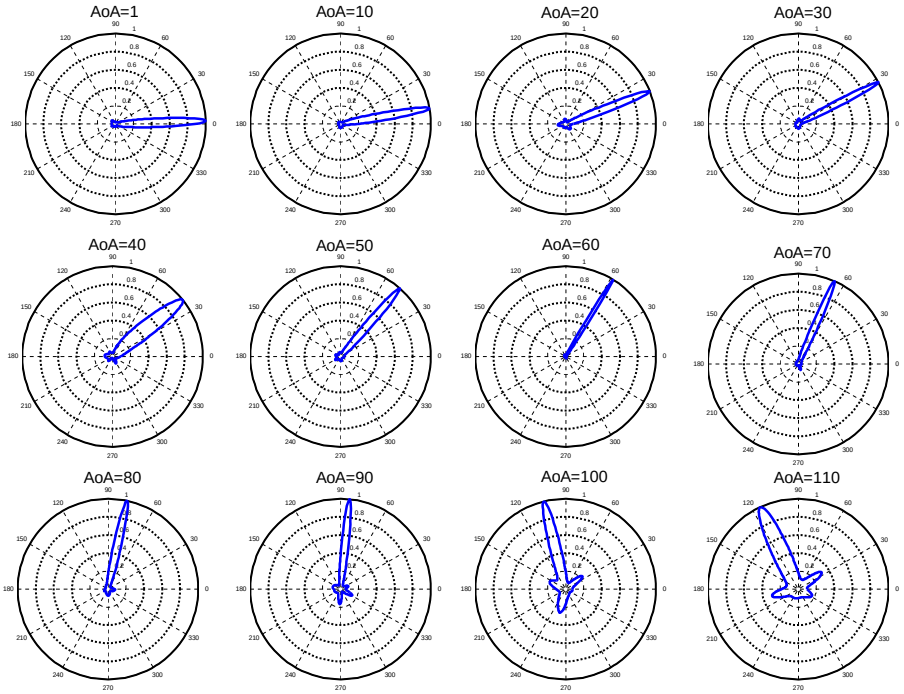

Figure 4.3: AoA results after using B matrix compensation (Position 1 to 110 at every 10 degree)

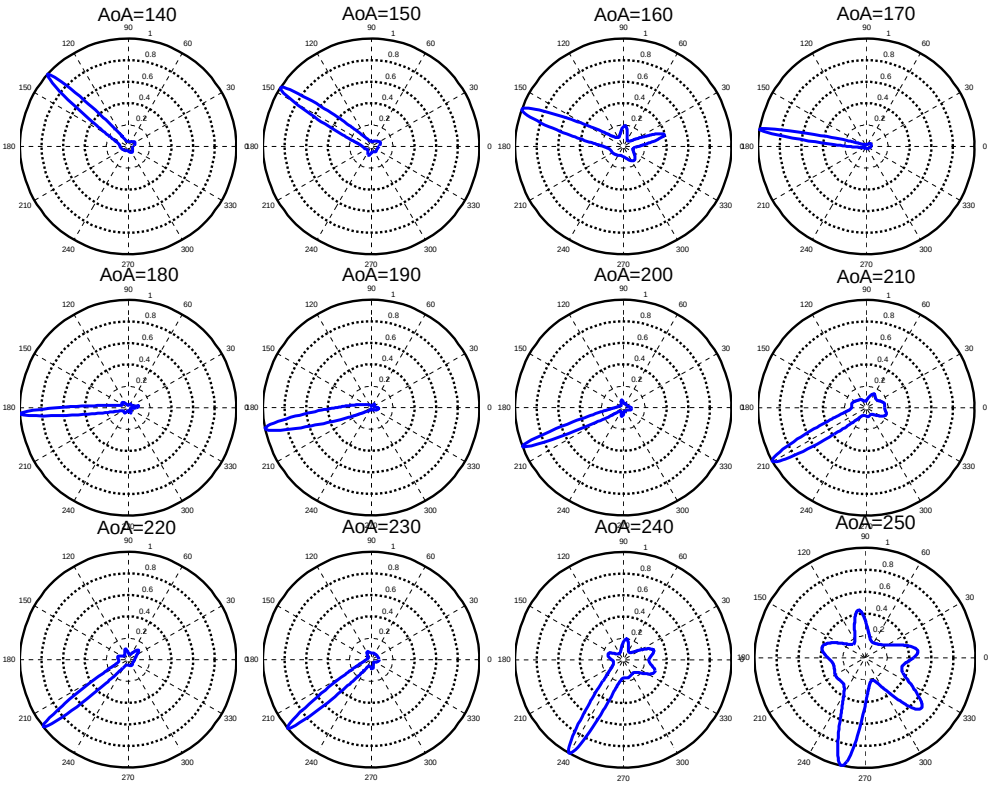

Figure 4.4: AoA results after using B matrix compensation (Position 140 to 250 at every 10 degree)

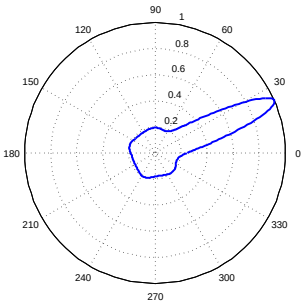

Figure 4.5: AoA=25 before using B matrix

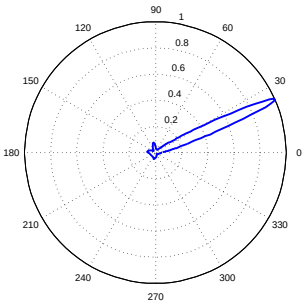

Figure 4.6: AoA=25 after using B matrix

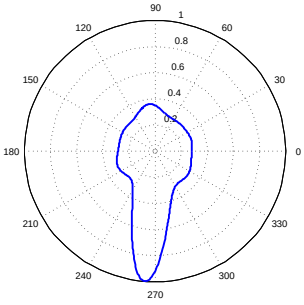

Figure 4.7: AoA=264 before using B matrix

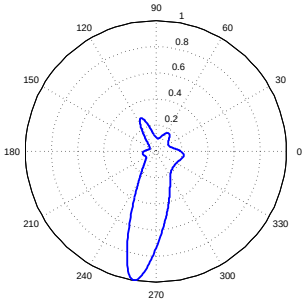

Figure 4.8: AoA=264 after using B matrix

positions, if some positions are not good enough, it will affect the result of B matrix. In order to find these not good enough positions, we use η *-score*. The purpose of η *-score* is to show that the score increases in the presence of peaks towards the true angle bearing , and decreases in the presence of peaks at bearing that is away from the true bearing. Here, Gaussian mask is used to compute the η *-score*, since Gaussian ensures that the AoA peaks close to the true bearing also get high η *-score*, which can tolerate small AoA estimation inaccuracies. In the experiment, we choose $\sigma^2 = 0.1$ for the Gaussian mask. The result of η *-score* for different positions is shown in Figure 4.9. It is clearly to see that positions around 250 degree have lower η *-score* than other positions. So we discard these positions, and use the remaining data to compute a new B matrix. Figure 4.10 and Figure 4.11

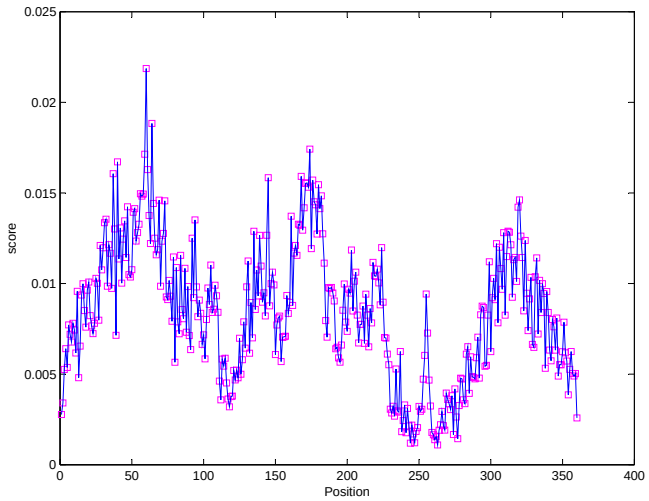

Figure 4.9: Score vs. Position

results show the AoA peak result before B matrix usage and after a new B matrix compensation. Figure 4.10 Before using B matrix, the AoA peak is wide and slight inaccurate. Figure 4.11 is the AoA result after using the new B matrix compensation, we can see now the peak is much sharper and angle is more accurate.

4.2 path cancellation

To evaluate the path cancellation method, we first run some simulations to see how the cancellation performs under different signal strength levels. We created two

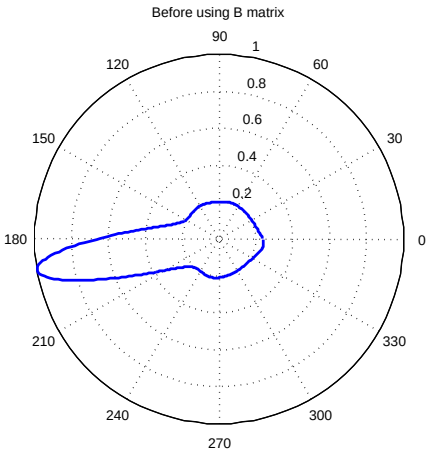

Figure 4.10: AoA before using B matrix

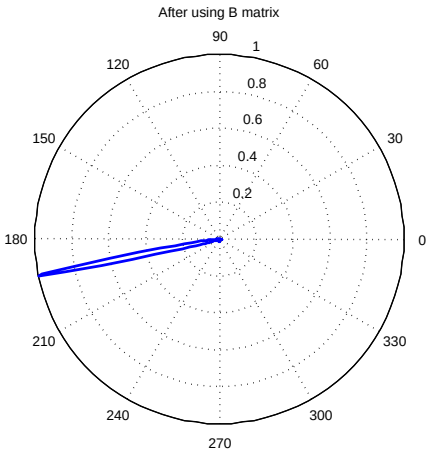

Figure 4.11: AoA after using new B matrix

signals from 30 and 60 degrees, and change their magnitude ratio in db. We would like to cancel 30 degree signal and keep 60 degree signal. From these results,we can see that even when the 60 degree is very weak (with a large magnitude ratio), the method still can cancel the much stronger signal and detect the weaker one. We

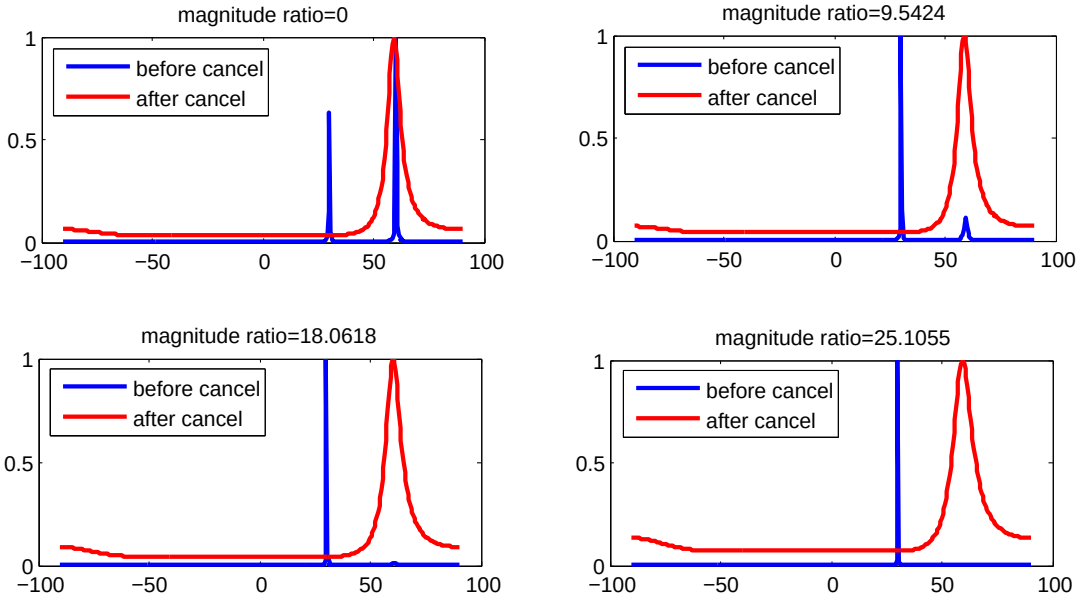

Figure 4.12: simulation Interference cancellation different signal strength level

also applied the method on real experiments. With one antenna transmits signal, a 8 element uniform circular array receives in indoor environment. Figure 4.13 shows that MUSIC detected two peaks, the large one is the direct path and the small one is the reflected path. Figure 4.14 is the result after we cancel the direct path, the

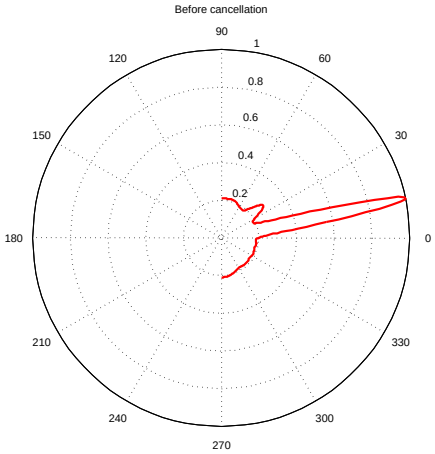

Figure 4.13: Before direct path cancel

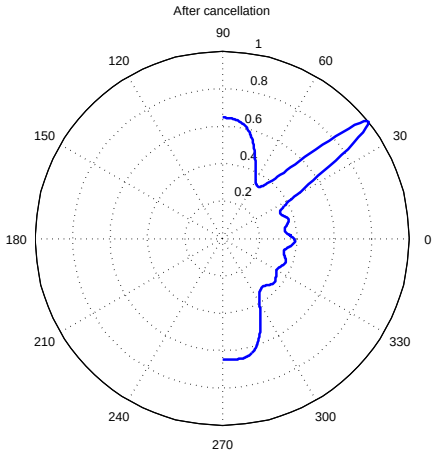

Figure 4.14: After direct path cancel

result is normalized. The result shows that the path cancellation method works well even when the reflected path signal strength is relatively small. This matches the simulation results.

Chapter 5

Conclusions

In this thesis, I have firstly comprehensively reviewed the existing wireless channel parameter estimate methods and discussed how the performance of the parameter estimate methods deteriorates significantly in the presence of array imperfections. To more accurately characterise wireless channel parameters, I have presented an experimental evaluation of an B matrix technique to compensate the effect of imperfection of the receiving antennas and radio hardwares, also a path cancellation technique has been combined to further improve the parameter estimation results.

The array imperfection effects are modeled in a radio anechoic chamber and B matrix result from experimental measurements in the anechoic chamber are then processed outside the anechoic chamber. Our AoA results show great improvement after the B matrix compensation. The efficacy of path cancellation technique has also been validated through Matlab simulation and experimental results in real-world environments, our results show that even in the situation that the signal which needs to be canceled is much stronger than the signal which needs to be keep, this path cancellation method can still successfully detects the weaker signal while cancels the stronger one.

Many practical applications, such as indoor localization, require the accurate parameter estimation results, thus this work has taken the array imperfection factors into account and shows how these parameter estimation results can be improved using a B matrix technique and path cancellation method.

Bibliography

[1] David Tse and Pramod Viswanath. *Fundamentals of Wireless Communication*. Cambridge University Press, New York, NY, USA, 2005.

[2] P. N. Fletcher, M. Dean, and A. R. Nix. Mutual coupling in multi-element array antennas and its influence on mimo channel capacity. *Electronics Letters*, 39(4):342–344, Feb 2003.

[3] J. Capon. High-resolution frequency-wavenumber spectrum analysis. *Proceedings of the IEEE*, 57(8):1408–1418, Aug 1969.

[4] C. Vaidyanathan and K. M. Buckley. Performance analysis of the mvdr spatial spectrum estimator. *IEEE Transactions on Signal Processing*, 43(6):1427–1437, Jun 1995.

[5] R. Schmidt. Multiple emitter location and signal parameter estimation. *IEEE Transactions on Antennas and Propagation*, 34(3):276–280, Mar 1986.

[6] A. Barabell. Improving the resolution performance of eigenstructure-based direction-finding algorithms. In *Acoustics, Speech, and Signal Processing, IEEE International Conference on ICASSP '83.*, volume 8, pages 336–339, Apr 1983.

[7] B. Friedlander. Direction finding using an interpolated array. In *Acoustics, Speech, and Signal Processing, 1990. ICASSP-90., 1990 International Conference on*, pages 2951–2954 vol.5, Apr 1990.

[8] A. B. Gershman and J. F. Bohme. A note on most favorable array geometries for doa estimation and array interpolation. *IEEE Signal Processing Letters*, 4(8):232–235, Aug 1997.

[9] A. J. Weiss and B. Friedlander. Performance analysis of spatial smoothing with interpolated arrays. *IEEE Transactions on Signal Processing*, 41(5):1881–1892, May 1993.

[10] P. Hyberg, M. Jansson, and B. Ottersten. Array interpolation and doa mse reduction. *IEEE Transactions on Signal Processing*, 53(12):4464–4471, Dec 2005.

[11] P. Hyberg, M. Jansson, and B. Ottersten. Sector array mapping: transformation matrix design for minimum mse. In *Signals, Systems and Computers, 2002. Conference Record of the Thirty-Sixth Asilomar Conference on*, volume 2, pages 1288–1292 vol.2, Nov 2002.

[12] M. A. Doron and E. Doron. Wavefield modeling and array processing .i. spatial sampling. *IEEE Transactions on Signal Processing*, 42(10):2549–2559, Oct 1994.

[13] M. A. Doron and E. Doron. Wavefield modeling and array processing .ii. algorithms. *IEEE Transactions on Signal Processing*, 42(10):2560–2570, Oct 1994.

[14] M. A. Doron and E. Doron. Wavefield modeling and array processing. iii. resolution capacity. *IEEE Transactions on Signal Processing*, 42(10):2571–2580, Oct 1994.

[15] F. Belloni, A. Richter, and V. Koivunen. Doa estimation via manifold separation for arbitrary array structures. *IEEE Transactions on Signal Processing*, 55(10):4800–4810, Oct 2007.

[16] F. Belloni, A. Richter, and V. Koivunen. Performance of root-music algorithm using real-world arrays. In *Signal Processing Conference, 2006 14th European*, pages 1–5, Sept 2006.

[17] F. Belloni, A. Richter, and V. Koivunen. Extension of root-music to non-ula array configurations. In *2006 IEEE International Conference on Acoustics Speech and Signal Processing Proceedings*, volume 4, pages IV–IV, May 2006.

[18] M. Rubsamen and A. B. Gershman. Direction-of-arrival estimation for nonuniform sensor arrays: From manifold separation to fourier domain music methods. *IEEE Transactions on Signal Processing*, 57(2):588–599, Feb 2009.

[19] Tie-Jun Shan, M. Wax, and T. Kailath. On spatial smoothing for direction-of-arrival estimation of coherent signals. *IEEE Transactions on Acoustics, Speech, and Signal Processing*, 33(4):806–811, Aug 1985.

[20] S. U. Pillai and B. H. Kwon. Forward/backward spatial smoothing techniques for coherent signal identification. *IEEE Transactions on Acoustics, Speech, and Signal Processing*, 37(1):8–15, Jan 1989.

[21] S. U. Pillai and B. H. Kwon. Performance analysis of music-type high resolution estimators for direction finding in correlated and coherent scenes. *IEEE Transactions on Acoustics, Speech, and Signal Processing*, 37(8):1176–1189, Aug 1989.

[22] B. Friedlander and A. J. Weiss. Direction finding using spatial smoothing with interpolated arrays. *IEEE Transactions on Aerospace and Electronic Systems*, 28(2):574–587, Apr 1992.

[23] N. Odachi, H. Shoki, and Y. Suzuki. High-speed doa estimation using beamspace music. In *Vehicular Technology Conference Proceedings, 2000. VTC 2000-Spring Tokyo. 2000 IEEE 51st*, volume 2, pages 1050–1054 vol.2, 2000.

[24] D. J. Yeom, S. H. Park, J. R. Kim, and M. J. Lee. Performance analysis of beamspace music with beamforming angle. In *Signal Processing and Communication Systems (ICSPCS), 2014 8th International Conference on*, pages 1–5, Dec 2014.

[25] H. B. Lee and M. S. Wengrovitz. Resolution threshold of beamspace music for two closely spaced emitters. *IEEE Transactions on Acoustics, Speech, and Signal Processing*, 38(9):1545–1559, Sep 1990.

[26] M. Kaveh and A. Barabell. The statistical performance of the music and the minimum-norm algorithms in resolving plane waves in noise. *IEEE Transactions on Acoustics, Speech, and Signal Processing*, 34(2):331–341, Apr 1986.

[27] T. Lo, J. Litva, and H. Leung. A new approach for estimating indoor radio propagation characteristics. *IEEE Transactions on Antennas and Propagation*, 42(10):1369–1376, Oct 1994.

[28] G. Morrison and M. Fattouche. Super-resolution modeling of the indoor radio propagation channel. *IEEE Transactions on Vehicular Technology*, 47(2):649–657, May 1998.

[29] Xinrong Li and K. Pahlavan. Super-resolution toa estimation with diversity for indoor geolocation. *IEEE Transactions on Wireless Communications*, 3(1):224–234, Jan 2004.

[30] Jie Xiong, Karthikeyan Sundaresan, and Kyle Jamieson. Tonetrack: Leveraging frequency-agile radios for time-based indoor wireless localization. In *Proceedings of the 21st Annual International Conference on Mobile Computing and Networking*, pages 537–549. ACM, 2015.

[31] R. Roy and T. Kailath. Esprit-estimation of signal parameters via rotational invariance techniques. *IEEE Transactions on Acoustics, Speech, and Signal Processing*, 37(7):984–995, Jul 1989.

[32] R. Roy, A. Paulraj, and T. Kailath. Estimation of signal parameters via rotational invariance techniques - esprit. In *Military Communications Conference - Communications-Computers: Teamed for the 90's, 1986. MILCOM 1986. IEEE*, volume 3, pages 41.6.1–41.6.5, Oct 1986.

[33] R. Roy, A. Paulraj, and T. Kailath. Esprit–a subspace rotation approach to estimation of parameters of cisoids in noise. *IEEE Transactions on Acoustics, Speech, and Signal Processing*, 34(5):1340–1342, Oct 1986.

[34] A. Paulraj, R. Roy, and T. Kailath. A subspace rotation approach to signal parameter estimation. *Proceedings of the IEEE*, 74(7):1044–1046, July 1986.

[35] A. L. Swindlehurst, B. Ottersten, R. Roy, and T. Kailath. Multiple invariance esprit. *IEEE Transactions on Signal Processing*, 40(4):867–881, Apr 1992.

[36] M. Srensen and L. De Lathauwer. Multiple invariance esprit for nonuniform linear arrays: A coupled canonical polyadic decomposition approach. *IEEE Transactions on Signal Processing*, 64(14):3693–3704, July 2016.

[37] N. D. Sidiropoulos, R. Bro, and G. B. Giannakis. Parallel factor analysis in sensor array processing. *IEEE Transactions on Signal Processing*, 48(8):2377–2388, Aug 2000.

[38] M. C. Vanderveen, C. B. Papadias, and A. Paulraj. Joint angle and delay estimation (jade) for multipath signals arriving at an antenna array. *IEEE Communications Letters*, 1(1):12–14, Jan 1997.

[39] A. J. van der Veen, M. C. Vanderveen, and A. Paulraj. Joint angle and delay estimation using shift-invariance techniques. *IEEE Transactions on Signal Processing*, 46(2):405–418, Feb 1998.

[40] M. I. Miller and D. R. Fuhrmann. Maximum-likelihood narrow-band direction finding and the em algorithm. *IEEE Transactions on Acoustics, Speech, and Signal Processing*, 38(9):1560–1577, Sep 1990.

[41] A. A. Ksienski and R. B. McGhee. A decision theoretic approach to the angular resolution and parameter estimation problem for multiple targets. *IEEE Transactions on Aerospace and Electronic Systems*, AES-4(3):443–455, May 1968.

[42] A. G. Jaffer. Maximum likelihood angular resolution of multiple sources. In *Circuits, Systems and Computers, 1985. Nineteeth Asilomar Conference on*, pages 68–72, Nov 1985.

[43] M. Wax and T. Kailath. Optimum localization of multiple sources by passive arrays. *IEEE Transactions on Acoustics, Speech, and Signal Processing*, 31(5):1210–1217, Oct 1983.

[44] S. K. Oh and C. K. Un. Simple computational methods of the ap algorithm for maximum likelihood localization of multiple radiating sources. *IEEE Transactions on Signal Processing*, 40(11):2848–2854, Nov 1992.

[45] J. A. Fessler and A. O. Hero. Space-alternating generalized expectation-maximization algorithm. *IEEE Transactions on Signal Processing*, 42(10):2664–2677, Oct 1994.

[46] A. J. Weiss and B. Friedlander. Array shape calibration using sources in unknown locations-a maximum likelihood approach. In *Acoustics, Speech, and Signal Processing, 1988. ICASSP-88., 1988 International Conference on*, pages 2670–2673 vol.5, Apr 1988.

[47] I. Ziskind and M. Wax. Maximum likelihood localization of multiple sources by alternating projection. *IEEE Transactions on Acoustics, Speech, and Signal Processing*, 36(10):1553–1560, Oct 1988.

[48] M. Feder and E. Weinstein. Parameter estimation of superimposed signals using the em algorithm. *IEEE Transactions on Acoustics, Speech, and Signal Processing*, 36(4):477–489, Apr 1988.

[49] B. H. Fleury, D. Dahlhaus, R. Heddergott, and M. Tschudin. Wideband angle of arrival estimation using the sage algorithm. In *Spread Spectrum Techniques and Applications Proceedings, 1996., IEEE 4th International Symposium on*, volume 1, pages 79–85 vol.1, Sep 1996.

[50] P. Ioannides and C. A. Balanis. Uniform circular arrays for smart antennas. *IEEE Antennas and Propagation Magazine*, 47(4):192–206, Aug 2005.

[51] Mati Wax and Jacob Sheinvald. Direction finding of coherent signals via spatial smoothing for uniform circular arrays. *IEEE transactions on antennas and propagation*, 42(5):613–620, 1994.

[52] Warp pproject.